UNIVERSITY OF CAMBRIDGE
Department of Engineering

Uplift Resistance of an Under-Reamed Pile Foundation

Hok Kiu Johnson Leung

Downing College

Supervisor: Professor Gopal Madabhushi

Group D

25 May 2016

I hereby declare that, except where specifically indicated, the work submitted herein is my own original work.

Signed ____ *Date* ____________________________

Technical Abstract

Under-reamed pile foundations are piles featuring local enlargement(s) along their length, designed to either increase the end-bearing capacity or to enhance the uplift resistance. In the current project, a single enlargement was assumed to be at the pile base. These piles have been widely used at sites where significant uplift is expected, hence the uplift behaviour of which must be understood in order to employ them in practice. However, the theory behind uplift resistance is relatively well understood for plate anchors, but not for under-reamed piles due to insufficient academic research. This is particularly severe for clayey soils as little research has ever been attempted due to the complexity of the problem and difficulties in model preparation. The main target of this project is thus to investigate the behaviour of such piles embedded in clay, and compare it to the similar problem in sand and relevant findings in existing literature.

Small scale displacement-controlled half-space tests at 1g along with subsequent Particle Image Velocimetry (PIV) analysis were performed to investigate the load-displacement response and failure mechanism geometry of smooth model plate anchor and 45° under-reamed pile subjected to uplift in homogeneous clay and dense sand. For clay, the test samples were classified as either soft or stiff relative to the range of sample consistencies used in this project.

Current test results indicated that the uplift load-displacement response of under-reamed piles in dense sand resembled the expected behaviour of such soil upon simple shearing, whereby the sand initially dilates, reaches a well-defined peak strength at a relatively small displacement, then softens post-peak towards a critical state. Post-failure instability due to the phenomenon of soil arching was noticeable. The associated failure mechanism was a well-defined truncated cone ruptured in shear accompanied by some local compaction immediately above the pile base.

For clay, five regimes of behaviour were identified, each characterised by various stages of the underlying failure mechanism. At small strains (regime 1), the capacity increased rapidly and the initial stiffness increased with undrained shear strength via an empirical power-law relation. Yielding (regime 2) then followed, mobilising large displacements towards the ultimate state (regime 3). The peak capacity was observed to increase with undrained strength described by another power-law relation. Up to this point, a growing localised plastic zone in the form of a peach-shaped bulb was observed around the pile base, together with suction generated beneath the base but lost at an early stage. Sudden drops in load due to the loss of suction at the breakaway state were observed for the plate anchor but not for the 45° under-reamed pile

because of the different base bottom profile, in which a flat surface of the former was more prone to abrupt breakaway. The loss of suction caused degradation in both stiffness and capacity by 44% and 22% respectively. For load-controlled scenarios a dynamic jump in displacement of at least 50% would occur during breakaway, which might cause excessive damage to any overlying structures. Subsequently, the post-peak capacity was found to decrease slightly towards a temporary plateau (regime 4), reflecting the initiation and extension of tension cracks at shallow depths starting from the rim of the pile base towards the soil surface. For stiff clays, faster crack propagation led to a steeper reduction in capacity. At very large displacements, the clay exhibited strain softening (regime 5) as the cracks became fully-developed reaching the soil surface. A concave conical wedge defined by these cracks was then stressed largely in flexure and lifted up, causing upheaval of the soil surface locally around the pile shaft. The softening behaviour of clay was often not captured by other tests, since these stress states were not possible to be attained if the test was load-controlled. Even for displacement-controlled tests, it was not uncommon to overlook this feature by underestimating the large displacement to failure of clay (up to 2 orders of magnitude greater than that of sand) such that the test equipment might have reached its limit in applying the required displacement during the tests.

Comparisons between results in clay and in sand revealed that the former exhibited a much higher degree of plasticity, as expected for purely cohesive soils compared to frictional, granular soils. The distinctively larger displacement to failure utilised in clay was made possible by the extensive plastic flow prominent in its failure mechanism, in contrast to shear rupturing in sand. Results also showed that for clay the failure mechanism for under-reamed piles was similar to that for plate anchors, and the mechanism was typically more complex than sand due to the development of base suction and tension cracks at shallow depths prematuring tensile failure of the clay.

Several generalised methods for predicting the ultimate uplift capacity of under-reamed piles embedded in clay were discussed and compared against current test results. The methods were found to be mostly suitable or conservative for stiff clays, but they tended to overestimate the capacity in soft clays. Consequently, all these methods have to be used with caution when designing under-reamed piles in soft clays. In light of the inadequate research in this subject and the existence of scale effects in the field, any full scale or centrifuge tests verifying the results of this project would provide further invaluable insights into the uplift resistance of under-reamed pile foundations.

Table of Contents

Technical Abstract i
Table of Contents 1
Nomenclature 3

1. Introduction 4
   1.1 Background and context 4
   1.2 Under-reamed pile foundations 4
   1.3 Motivation for work 6
   1.4 Problem definition 6
   1.5 Aims and objectives 6

2. Literature Review 7
   2.1 Uplift capacity of under-reamed pile foundations in homogeneous sand 7
      2.1.1 Theoretical models 7
      2.1.2 Experimental studies 7
   2.2 Uplift capacity of plate anchors in homogeneous clay 8
      2.2.1 Theoretical models 8
      2.2.2 Experimental studies 9
   2.3 Uplift capacity of under-reamed pile foundations in homogeneous clay 9
      2.3.1 Theoretical models 9
      2.3.2 Experimental studies 10
   2.4 Failure mechanism characterisation 11
      2.4.1 Sand 11
      2.4.2 Clay 12

3. Experimental Apparatus and Methodology 13
   3.1 Test container 13
   3.2 Soils used 14
      3.2.1 Sand 14
      3.2.2 Clay 14
   3.3 Model piles 15
      3.3.1 Specification 15
      3.3.2 Installation 15
   3.4 Equipment 16
   3.5 Instrumentation 17
      3.5.1 Load measurement 17
      3.5.2 Displacement measurement 17
      3.5.3 Data acquisition 18
   3.6 Data processing 18
   3.7 Full experimental set-up 19
   3.8 Experimental procedure 19
   3.9 Test schedule 20
   3.10 Experimental accuracy 21

4. Pile Load-Displacement Response ... 22
4.1 Experimental results ... 22
4.1.1 Comparison between soft and stiff clays ... 23
4.1.2 Comparison between under-ream angles ... 24
4.1.3 Comparison between sand and clay ... 25
4.2 Comparison to literature ... 26
4.2.1 Load-displacement curve form ... 26
4.2.2 Ultimate uplift resistance ... 27
4.2.3 Post-failure strain softening of clay ... 29
4.2.4 Post-failure arching and instability of sand ... 30

5. Soil Failure Mechanism Characterisation ... 31
5.1 Plate anchor ... 31
5.1.1 Soft clay mechanism ... 31
5.1.2 Stiff clay mechanism ... 32
5.1.3 Comparison to literature ... 33
5.2 Under-reamed pile (45°) ... 34
5.2.1 Soft clay mechanism ... 34
5.2.2 Stiff clay mechanism ... 35
5.2.3 Dense sand mechanism ... 36
5.2.4 Comparison between dense sand and soft/stiff clay mechanisms ... 37
5.2.5 Comparison to literature ... 38

6. Theoretical Predictions ... 41
6.1 Theoretical model by Meyerhof & Adams (1968) and its variants ... 41
6.2 Estimation procedure by Das (1980) ... 42
6.3 3D lower bound solutions by Merifield et al. (2003) ... 43
6.4 Analytical equation by Golait et al. (2014) ... 43
6.5 Comparison with experimental results ... 44

7. Conclusions ... 45

8. Recommendations for Future Work ... 46

References ... 47
Appendix: Risk Assessment Retrospective ... 50

Hok Kiu Johnson Leung
Downing College

Nomenclature

A	Projected plan area of the under-ream base [m^2]
B	Pile base diameter [m]
B_s	Pile shaft diameter [m]
c	Soil cohesion [kPa]
c_u	Undrained shear strength [kPa]
D	Embedment depth of pile measured from soil surface to point of widest diameter (the datum level) [m]
e_{max}	Maximum voids ratio [-]
e_{min}	Minimum voids ratio [-]
I_D	Relative density [-]
N_{qu}	Non-dimensional uplift capacity [-]
Q_u	Ultimate uplift capacity [N]
γ	Soil unit weight [kN/m^3]
δ	Pile head displacement [m]
θ	Pile under-ream angle measured from the horizontal [°]
ϕ	Soil internal friction angle [°]
ϕ_{crit}	Critical state internal soil friction angle [°]

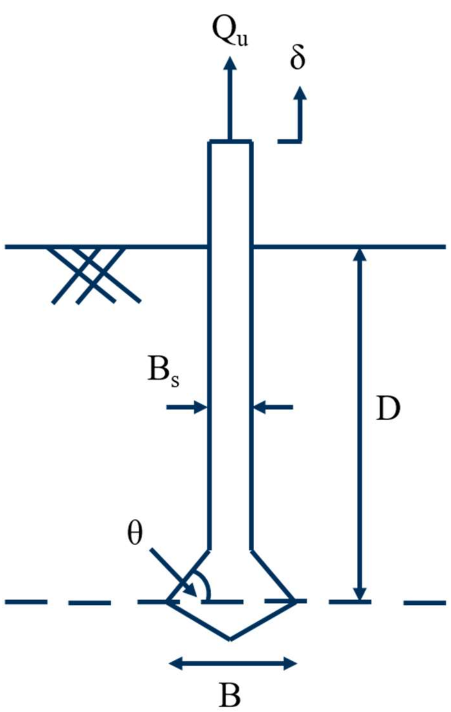

Figure (i): Schematic illustrating key parameters

1. Introduction

1.1 Background and context

Civil structures aboveground are often supported by load transfer to the subsurface through foundations. These loads are mostly compressive due to the self-weight of the structure. However, foundation loads can be tensile under certain conditions, and the foundation in turn exerts an uplift force to the surrounding soil. Situations in which this can occur include:

- Lightweight steel frame structures (e.g. transmission pylons) subjected to high lateral wind loading, inducing large overturning moments at the foundation level in the form of tensile and compressive forces on the windward and leeward sides of the foundation respectively.
- Anchored offshore structures (e.g. oil platforms) subjected to dynamic wave loading and buoyancy forces, again causing large moments and uplift forces.
- Sites with expansive soils (e.g. Black Cotton Soil in India), the swelling of which due to an increase in moisture content results in an uplift force on the foundation. In particular, Black Cotton Soil undergoes significant volumetric strains upon seasonal moisture changes, leading to potentially excessive ground deformations.

In such conditions, piled schemes tend to be more economical than conventional large gravity based foundations (Hopkins, 2012). This would require piles to have adequate capacities in resisting the uplift forces. Pile under-reaming turns out to be a viable solution in terms of performance, cost and materials.

1.2 Under-reamed pile foundations

Under-reamed pile foundations are piles featuring local enlargement(s) along their length, designed to either increase the end-bearing capacity or to enhance the uplift resistance by mobilising a passive soil wedge at failure (Figure 1). Also known as 'mushroom foundations' (Balla, 1961) and 'belled piers' (Dickin & Leung, 1990), these piles are a subset of bored piles (or drilled shafts). The geometry of the enlargement is usually in the form of an inverted cone at the base, but can also be one or more intermediate bulbs along the pile shaft. In the present study, the former type of pile geometry is assumed.

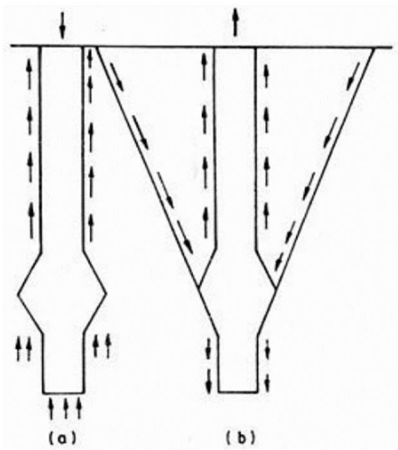

Figure 1: Load transfer mechanism for under-reamed piles
(a) compressive load (b) tensile load
(Gupta, 1986)

The under-ream can be formed in-situ by rotating a hinged belling bucket at the end of the drill stem on a rotary drilling rig inside a pre-drilled straight shaft (Figure 2 & Figure 3), or by placing a precast element in an existing excavated pit prior to backfilling and compaction (Balla, 1961). An additional 75-100% load carrying capacity can be attained for cast in-situ concrete piles by driving the reinforcement cage down through the freshly poured concrete, thereby forcing the concrete to flow laterally into the enlargement and compacting the whole pile mass. The resulting pile system is known as a ‘bored compaction pile’ (Jain et al., 1975).

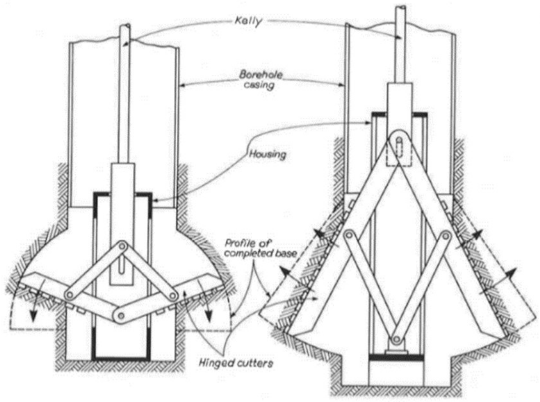

Figure 2: Under-reaming tools (Tomlinson, 2001)

Various research has demonstrated that under-reamed piles are superior to other traditional foundation systems in many aspects, including the provision of uplift resistance in the scenarios described in section 1.1 (Gupta, 1986). These piles are particularly cost-effective for sites comprising of soft soils, expansive clays or weak soils underlain by strong soils, where the under-ream acts as an anchor at great depth in a relatively stable stratum and thus limits any large differential settlements at ground level that may cause unacceptable cracking and damage to the overlying structure. Together with their speed and ease of construction, an overall saving of 30-60% in cost compared to strip or ordinary pile foundations can be achieved (Mohan, 1989).


Figure 3: Top-hinged under-reaming bucket (Tomlinson, 2001)

Practical design and construction of under-reamed piles are codified in the Indian Standard IS 2911-3 (Bureau of Indian Standards, 1980), which suggests the ultimate uplift capacity of a singly under-reamed pile in clayey soils can be predicted by the normal bearing capacity equation, but with the assumption that only the enlargement (but not the pile stem) is end-bearing. Consequently, omitting the pile tip bearing term while keeping all other terms unchanged implies no distinction being made between the failure mechanisms of bearing and uplift. Similar guidelines are also given in the U.S. design manual for drilled shafts (Reese & O’Neill, 1999). Overall considerations on the usage of under-reamed piles are covered by Sharma et al. (1978) and Varghese (2009).

1.3 Motivation for work

There has been a widespread use of under-reamed piles nowadays in industry. Although not commonly found in the UK, under-reamed piles are predominantly employed in India, South East Asia (Harris & Madabhushi, 2015) and along the Texas Gulf Coast (Tand et al., 2005). In these practical situations, foundations must be designed to satisfy safety and serviceability criteria, and remain economical at the same time. Hence, the behaviour of under-reamed piles must be understood. However, the theory behind uplift resistance is relatively well understood for plate anchors, but not for under-reamed piles due to insufficient academic research. This is particularly severe for clayey soils as little research has ever been attempted. The main target of this project is thus to investigate the behaviour of such piles embedded in clay. It is the inadequacy of academic research coupled with the high applicability of under-reamed piles in practice that drives the current project to explore the frontiers of this subject.

1.4 Problem definition

This project is a natural extension of the work done by Hopkins (2012), Harris (2014) and Hughes (2015), who examined the problem in sandy soils. In the present project, small scale displacement-controlled half-space tests at 1g were conducted to investigate the load-displacement response and failure mechanism geometry of smooth model plate anchor and 45° under-reamed pile subjected to uplift in homogeneous clay stratum. This research forms a comparative study but does not aim towards predicting the behaviour of fully sized piles in the field due to significant differences in soil confining stress. In addition, upward displacement at SLS (being much less than that at ULS) often governs the design of under-reamed piles under uplift in practice (Xu et al., 2012).

1.5 Aims and objectives

The primary intentions of this project were:

- To examine the load-displacement response of under-reamed piles in clay (and in dense sand as a trial) by conducting small scale pullout tests on half-space model piles at 1g.
- To characterise the underlying failure mechanism using particle image velocimetry (PIV), a technique which tracks soil movements via digital imaging.
- To contrast the observed uplift behaviour of under-reamed piles in clay and in sand.
- To review relevant findings in existing literature and compare the experimental results to them.

2. Literature Review

2.1 Uplift capacity of under-reamed pile foundations in homogeneous sand

There has been a great amount of investigation on the uplift resistance of plate anchors in sand, but comparatively fewer studies have considered the more general under-ream geometries. Historical findings presented in this section are mostly related to under-reamed (belled) piles, yet some important milestones on the development of plate anchor theory are also highlighted.

2.1.1 Theoretical models

Balla (1961) was one of the pioneers in studying the uplift resistance of transmission tower foundations in the form of piles with enlarged bases. A semi-analytical formula for the ultimate uplift capacity of under-reamed piles was established using Kötter's equation and results from small scale model tests at 1g, which was found to predict the ultimate capacity of full scale test piles reasonably well. Meyerhof & Adams (1968) laid the cornerstone for the development of plate anchor theory by proposing a generalised theoretical framework for the problem based on an idealised failure model of soil and compare it with laboratory and field test results. This conceptual model divides the anchor behaviour into two regimes depending on whether the failure surface reaches the surface – the anchor is regarded as 'shallow' if so, otherwise it is considered 'deep' (Figure 4). It was found that the uplift capacity increased with embedment until a critical embedment ratio ($\frac{H}{D}$ as defined in Figure 4) was reached (Meyerhof & Adams, 1968; Dickin, 1988; Ilamparuthi et al., 2002). This reflected the transition of anchor behaviour from shallow to deep, thus was in alignment with the proposed theory. Murray & Geddes (1987) initiated the use of a normalised uplift capacity $N_{qu} = \frac{Q_u}{\gamma AD}$ which was widely adopted in subsequent literature.

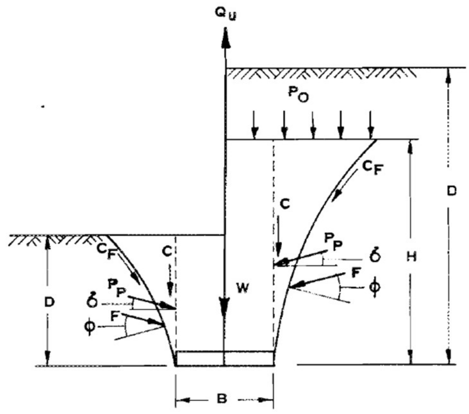

Figure 4: Failure surface of a plate anchor under uplift load (Meyerhof & Adams, 1968)

2.1.2 Experimental studies

An extensive model test programme with two sets of tests had been conducted by Dickin & Leung (1990; 1992) to investigate the uplift behaviour of under-reamed piles in sand. The first set of tests comprised of centrifuge model tests aimed at understanding the effect of embedment, under-ream size and soil properties on the problem (Dickin & Leung, 1990). As for plate anchors, the uplift capacity of under-reamed piles was found to increase with embedment and sand density. The load-displacement response in dense sand consisted of a well-defined peak followed by post-peak reduction. In loose sand, the load increased steadily towards a plateau at maximum level. This reflected the expected behaviour of sand under direct shearing, where dense and loose sands exhibit dilative and contractile behaviour respectively. The effect of under-ream angle on the problem was investigated via another set of centrifuge model tests (Dickin & Leung, 1992). The finding was that the uplift capacity decreased upon an increase in under-ream angle, and this being especially apparent for under-ream angles larger than 62°.

Recent investigations on the uplift resistance of under-reamed piles in sand include small scale model tests at 1g performed by Hopkins (2012), Harris & Madabhushi (2015) and Hughes (2015). All had common observations regarding the pile load-displacement response as those made by Dickin & Leung (1992) described above, but were inconsistent with the results for plate anchors obtained by Ilamparuthi et al. (2002) as explained in section 4.2.1. For the influence of under-ream angle, Harris & Madabhushi (2015) deduced that the pullout capacity decreased monotonically with increasing under-ream angle in loose sand, while in dense sand an under-ream angle of about 45° - $\frac{\phi}{2}$ gave the highest uplift capacity. Post-failure instability due to sand arching (section 4.2.4) was widely observed (Murray & Geddes, 1978; Dickin, 1988; Ilamparuthi et al., 2002; Hopkins, 2013; Harris & Madabhushi, 2015; Hughes, 2015).

2.2 Uplift capacity of plate anchors in homogeneous clay

2.2.1 Theoretical models

Meyerhof & Adams (1968) attempted to apply their plate anchor theory (simplified into a cylindrical failure surface projected up above the plate) in clay. They foresaw that at large depths the flexing of the clay mass within the failure surface would be inhibited by the weight of the overburden, hence an empirical procedure related to the undrained strength c_u of the clay was suggested for estimating the ultimate uplift capacity (section 6.1). This approach was analogous to the bearing capacity equation suggested by Meyerhof (1951) in that the uplift coefficient N_u increased with depth up to a value of 9 (which was identical to the undrained bearing capacity factor N_c in clay) for deep anchors, a result agreed subsequently by model tests conducted by Das (1978). Numerical results presented by Merifield et al. (2003) reflected essentially the same concept, but with the notion that an anchor could be shallow or deep at a given embedment depending on the normalised overburden ratio $\frac{\gamma D}{c_u}$. Vesic (1971) on the other hand proposed an analytical method for estimating the pullout capacity of anchors embedded in clay using cavity expansion theory. In his method, the ultimate pullout capacities for strip and circular anchors were taken to be the pressures required to breakout a cylindrical and spherical cavity at a certain depth respectively plus the weight of soil above the anchor.

Rowe & Davis (1982) and Merifield et al. (2003) performed rigorous numerical analyses investigating the effect of shape upon the undrained uplift capacity of plate anchors in clay. The former used an elasto-plastic finite element analysis to obtain an expression for the shape factor of a circular anchor in terms of the embedment ratio. The latter used 3D lower bound limit analysis to quantify the ultimate uplift capacities of anchors with different shapes assuming no suction (section 6.3). These analyses were done because plane strain conditions were deemed to be unrealistic in the field (Singh & Ramaswamy, 2008).

2.2.2 Experimental studies

Upon comparison with their own model test results (corrected for suction), Meyerhof & Adams (1968) discovered that their cylindrical theory predicted the uplift capacity well at great depths, but overestimated at shallow depths by about 50%. This discrepancy for shallow anchors was thought to be due to the relatively large deformation to failure occurred in the clay. As the anchor became shallower, the formation of tension cracks prematured tensile failure of the clay.

Based on previous model test results (mostly on soft clays) of Das (1978) and others, Das (1980) proposed a general procedure to estimate the ultimate uplift capacity of plate anchors in clay excluding suction effects (section 6.2). Chaudhuri & Symons (1986) and Singh & Ramaswamy (2008) also conducted relevant model tests to reveal the approximately elasto-plastic load-displacement behaviour of the anchor, whereby a rapid increase in load was observed before reaching a plateau at maximum load. The former researchers found that the Meyerhof & Adams (1968) method offered the closest prediction to their test results.

Most researchers have acknowledged and attempted to quantify the salient features of the behaviour of clay observed from tests. These include the development of tension cracks at shallow depths (Meyerhof & Adams, 1968; Sutherland, 1988) and base suction (Meyerhof & Adams, 1968; Vesic, 1971; Lehane et al., 2008; Singh & Ramaswamy, 2008).

2.3 Uplift capacity of under-reamed pile foundations in homogeneous clay

Distinctively few researchers have considered extending the problem of uplift behaviour of foundations in homogeneous clay to under-reamed piles from the case of plate anchors.

2.3.1 Theoretical models

Having realised the inadequacy of research into the subject, Golait et al. (2014) established an analytical equation for computing the ultimate uplift capacity of under-reamed piles in soft to medium clays, which was derived from an assumed load transfer failure mechanism (section 6.4). A set of load-controlled model tests was conducted to verify the prediction. The method was found to have an error no more than 15% for $\frac{D}{B_s} > 8$, but up to 40% for $\frac{D}{B_s} < 8$. Difficulty in locating the ultimate state from the resulting load-displacement plots was claimed, together with the fact that surface upheaval and cracks were not observed during the tests, it was likely that the ultimate state had not been attained in the tests.

Sakajo et al. (1995) employed the finite element method to back-analyse centrifuge test results of model belled piles in cohesive soil. It was found that both elasto-plastic and elasto-viscoplastic FE models were conservative or suitable for over-consolidated clays, but they overpredicted the uplift resistance in normally-consolidated clays for reasons unclear at the time. Results also indicated the uplift resistance decreased with increasing under-ream angle (from 14.0° to 26.5°). Chai et al. (2005) were one of the first to realise the need to consider strain softening behaviour of clays in the context of under-reamed piles under uplift. Finite element analyses based on the Modified Cam clay (MCC) model were conducted. Comparison with results from a 60g centrifuge test revealed that uplift resistance greatly decreased with strain softening, stiffer clays required smaller displacement to mobilise peak resistance and exhibited a greater degree of softening for a given displacement. Results also showed that the existence of base suction significantly enhanced the uplift capacity (by 50% in their case), a view also shared by Thorne et al. (2004).

When expansive soils are being encountered, this opens up a whole stream of research possibilities regarding the uplift resistance of under-reamed piles in such soils. Poulos & Davis (1980) performed an elastic analysis of under-reamed piles in expansive clays and deduced that founding the piles just underneath the bottom of the active swelling zone would effectively control pile displacements induced by swelling of soil. However, this was disagreed by others in that the active zone capacity should be neglected to ensure safe design (Gupta, 1986).

2.3.2 Experimental studies

Limited research was conducted on this subject. Rattley et al. (2008) performed centrifuge tests on model tower footings in clay to examine the effect of suction and rate of loading upon the uplift capacity. They deduced that the uplift stiffness and capacity of the pile were strongly dependent on rate which in turn affected the dissipation of base suction during loading. This was complemented by centrifuge tests conducted by Lehane et al. (2008) on model footings in clay backfilled by sand. Base suction generated was found to increase with the rate of applied displacement v_f due to reduced drainage during load application. A normalised velocity $V = \frac{v_f B}{c_v}$ was defined for assessing any partial suction generated under a constant v_f.

Su et al. (2006) investigated the uplift behaviour of transmission tower foundations in expansive soils by constructing and testing (in a load-controlled manner) small scale and fully sized prototype models in the field, followed by a FE analysis to examine the failure mechanism. The elasto-plastic load-displacement behaviour of these under-reamed piles was explained using the underlying failure mechanism. It was also emphasised that simple scaling of results obtained among models (even of similar sizes) was inappropriate due to scale effects.

2.4 Failure mechanism characterisation

It is widely accepted that the uplift resistance of plate anchors originates from the shear resistance mobilised along the failure surface together with the weight of soil (and pile) contained within the mechanism. Again, limited research has been carried out to extend the problem to the more general case of under-reamed piles. Even for the case of plate anchors, there has been no consensus upon a generic theory of uplift resistance. This was thought to be caused by difficulties in characterising the underlying failure mechanism geometry (Meyerhof & Adams, 1968; Murray & Geddes, 1987; Ilamparuthi et al., 2002).

2.4.1 Sand

Ilamparuthi et al. (2002) performed half space model tests on plate anchors attempting to visualise soil failure and also reviewed existing failure mechanism geometries proposed by other researchers among which three main geometries were emphasised for shallow anchors – namely the vertical slip surface model (VSSM), the truncated soil cone model and the circular arc model (Figure 5), the last of which was originally proposed by Balla (1961). They discovered both the VSSM and soil cone model were conservative. Dickin (1988) evaluated the VSSM and also found that it was immensely conservative. On the contrary, Harris & Madabhushi (2015) found that the uplift resistances predicted by Meyerhof & Adams (1968) for a plate anchor assuming both the VSSM and soil cone model were unconservative for small scale model under-reamed piles. For deep anchors, the failure mechanism geometry is not very well understood yet. Nonetheless, "balloon shaped" mechanisms symmetrical about the anchor axis had been observed by Ilamparuthi et al. (2002) and Harris & Madabhushi (2015).

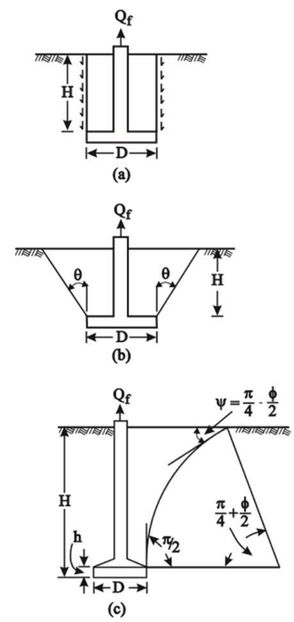

Figure 5: Assumed failure surfaces for shallow anchors (a) vertical slip surface model (b) truncated soil cone model (c) circular arc model (Ilamparuthi et al., 2002)

In their half space model tests on under-reamed piles at 1g, Dickin & Leung (1992) observed that failure was confined to the under-ream-sand interface in loose sand. In dense sand, an incomplete rupture plane was seen to be much less developed than previous results on plate anchors (Meyerhof & Adams, 1968; Dickin, 1988). Similar half space model tests and PIV analysis on under-reamed piles conducted by Harris & Madabhushi (2015) indicated that the failure mechanism was dependent on both the under-ream angle and sand density. The former was found to affect the failure mechanism locally around the pile base. For the latter, in dense sand a conical mechanism with extra zones of cavity expansion was observed. In loose sand, the “balloon shaped” (deep) mechanism failed to reach the soil surface due to local compaction around the under-ream. This was in contrast to the concept of “critical embedment ratio” suggested by Meyerhof & Adams (1968).

2.4.2 Clay

The failure mechanism in clay is more complex than that in sand due to the formation of tension cracks at shallow depths (Meyerhof & Adams, 1968). Thorne et al. (2004) proposed a set of possible uplift failure mechanisms for plate anchors in clays (Figure 6). These mechanisms were comprehensive in that they distinguished between shallow and deep behaviour with or without base suction. Merifield et al. (2003) also suggested failure mechanism geometries categorised as shallow and deep but with negligible suction. These were a subset of the mechanisms given by Thorne et al. (2004) except for shallow depths a concave conical variant was also suggested. Another set of geometries was presented by Tucker (1988) for belled piers according to embedment (Figure 7). Although aimed at modelling partly cohesive (c-ϕ) soils, Xu et al. (2012) performed finite element analyses to obtain axisymmetric, peach-shaped plastic zone contours for the uplift of deep under-reamed piles mainly under SLS (small strain) conditions and fitted the results with logarithmic spiral functions (Figure 8). This failure model had been used to develop a method for predicting the uplift resistance of such piles (Xu et al., 2009).

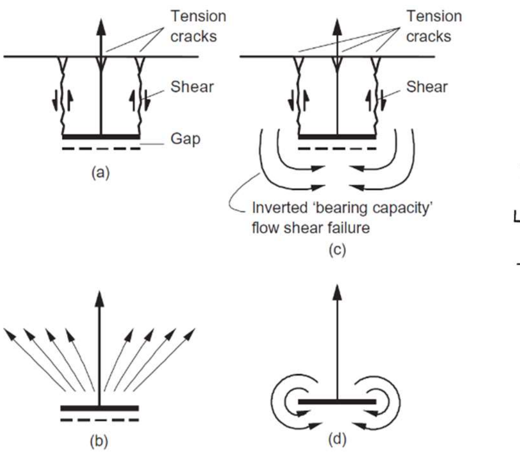

Figure 6: Uplift failure mechanisms in clay
(a) shallow anchor, separated from soil beneath
(b) shallow anchor, joined to soil beneath
(c) deep anchor, separated from soil beneath
(d) deep anchor, joined to soil beneath
(Thorne et al., 2004)

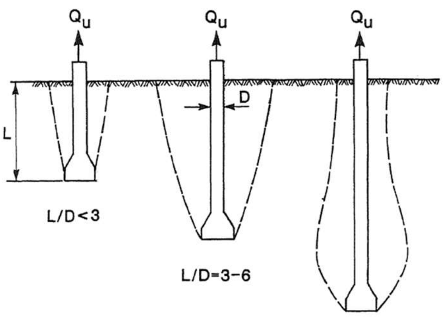

Figure 7: General failure modes for belled piers (Tucker, 1988)

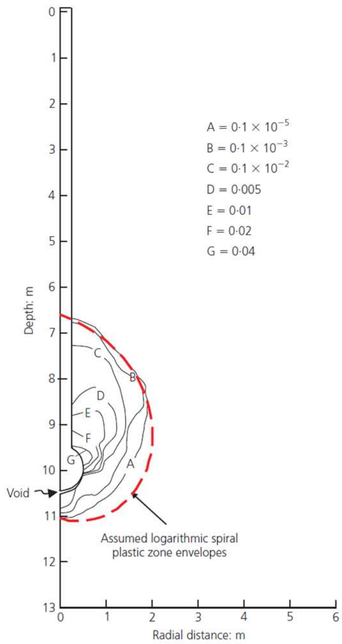

Figure 8: Cumulative plastic strain contours for cohesive soil in uplift at SLS (Xu et al., 2012)

3. Experimental Apparatus and Methodology

Unlike previous investigations, the current project involved only one type of test – half space model pile tests – in place of standard pullout tests that utilise full 3D model piles. This was due to the scarce amount of clay samples available for testing plus the tight time constraint imposed on the project. The half space tests were performed to give insights into both the load-displacement behaviour and the underlying failure mechanism geometry for a smooth plate anchor and 45° under-reamed pile in homogeneous clay (and dense sand).

3.1 Test container

The tests were conducted using a small sized timber container, measuring approximately 300 mm long, 300 mm wide and 150 mm deep. The container front face was a detachable, transparent perspex window. The choice of the small box size was a direct consequence of the limited supply of clay samples. Not a single block of clay given was large enough to fill up the entire enormous container (with dimensions of 705 x 300 x 500 mm^3) used in previous projects (Harris, 2014; Hughes, 2015). Further modifications to the box were deemed necessary for some tests in order to accommodate the relatively small blocks of clay (Figure 9). Despite of this, the box size was still thought to be great enough to allow one pile to be tested at a time without interference by the container edges, as confirmed by the PIV results.

Figure 9: Extra wooden boards fixed to test container (with perspex front face removed)

A uniform grid of 35 mm tall, 40 mm wide PIV control marker layout was adopted on the perspex screen. This easy-to-construct layout fulfilled the minimum PIV software requirement of 16 points without the need to presume the form of the mechanism and locations of the active shear bands. It consisted of 48 points (>>16 points) which should provide adequate redundancy against overlapping over the mechanism zone and capture far-field boundary effects (if any). Markers remaining in the mechanism zone served to maintain accurate calibration within that area.

3.2 *Soils used*

3.2.1 Sand

Table 1: Properties of Hostun HN31 sand (Mitrani, 2006)

Property	Value
e_{max} [-]	1.01
e_{min} [-]	0.555
ϕ_{crit} [°]	33
D_{50} [mm]	0.35

The first test was performed in dry Hostun HN31 sand, which was readily available at the Schofield Centre and relatively easy to handle. Table 1 shows the properties of Hostun HN31 sand assumed for this test, as the parameters were determined for the same soil species in the same laboratory (Mitrani, 2006). A mix of blue-dyed and standard species in a 1:10 ratio was used to increase the amount of texture in the images taken, so that the possibility of PIV tracking failures was reduced. A relative density of $I_D \approx 70\%$ (perceived in this project as 'dense') and a unit weight of $\gamma = 15.36$ kN/m^3 were attained in this test.

Preparation of the sand model involved sand pouring using a manual sand pourer. The drop height and nozzle diameter were adjusted to achieve the desired relative density. Adopting an oscillatory pouring pattern suggested by Harris (2014) to produce a uniform stratum, the sand pouring process was done in layers of 35 mm thickness (aligning the control points in elevation). For each layer, a thin stream (approximately 3 mm thick) of blue Hostun HN31 sand was poured against the perspex screen for rough visualisation of the failure mechanism without PIV analysis. This method has been the only way to visualise the failure mechanism geometry for some previous researchers (Balla, 1961; Dickin & Leung, 1992).

3.2.2 Clay


Figure 10: Hand vane shear test to find c_u of clay

The remaining four tests were performed in Kaolin clay with varying intrinsic properties and stress histories. It is important to note that there had been no control over the properties of clay samples, as they were supplied externally by other researchers in the laboratory rather than being reconstituted from scratch. Nevertheless, certain properties could be measured using relatively simple techniques. Undrained shear strength c_u of clay was evaluated via a hand vane shear test (Figure 10), found to be ranging from 10.45 kPa to 19.00 kPa. These limits were then perceived in this project as 'soft' and 'stiff'. By weighing and estimating the volume of clay the unit weight γ was found to fall within 15.79 kN/m^3 – 16.78 kN/m^3.

Preparation of the clay model involved detachment of the perspex window, followed by fitting the clay block (cut to a volume roughly similar to the box interior) into the open-faced box and minimising any potential gaps between the clay and the container at the same time. Any clay protruding from the open face was sliced off, giving a smooth uniform clay surface that was flush with the open face and in contact with the subsequently reinstalled perspex screen.

3.3 Model piles

3.3.1 Specification

The half space model piles were identical to those used by previous projects (Harris 2014; Hughes, 2015). Machined from Dural aluminium alloy, the surfaces of these piles were idealised to be perfectly smooth. The pile stems featured a rectangular cross-section for easy fabrication, and were 400 mm long, 12.7 mm wide and 7.2 mm thick. The widest diameter of the under-ream base was fixed at 60 mm (Figure 11). Two variants of the enlarged base were available – under-reams with angles of θ = 0° (effectively a plate anchor) and θ = 45° (Figure 12). A layer of PTFE tape was attached to the flat face of both piles to reduce friction at the pile-perspex interface. In view of the small applied loads expected in the current tests, the pile stem was assumed to be inextensible, and the whole pile system was considered to be perfectly rigid.

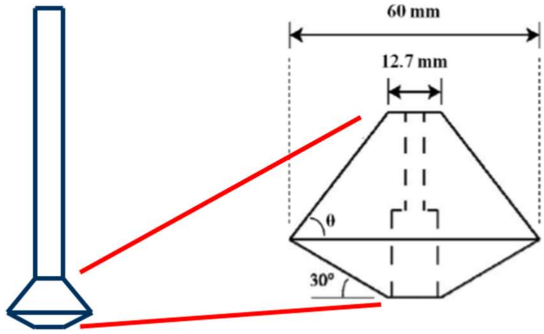

Figure 11: Model under-ream base geometry (after Harris, 2014)


Figure 12: Half space model piles plate anchor (above); 45° under-ream (below)

3.3.2 Installation

Installing model piles in sand mainly involved securing the pile in place using a D-clamp and mask tape, then pouring sand into the container and removing the tape and clamp sequentially as sand gradually filled up the box (Figure 13). A coat of silicon grease was smeared onto the PTFE tape on the flat pile face to seal off any gaps present in between the pile and perspex, hence preventing sand ingress during model preparation.

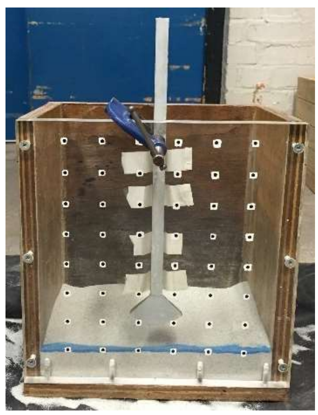
Figure 13: Model pile installation in sand


Figure 14: Model pile installation in clay

To install model piles in clay, the pile was simply pushed into the clay (with the flat side facing upwards) at the desired position on the exposed clay surface until the flat side of the whole pile levelled with the surrounding clay (Figure 14). Blue Hostun sand was sprinkled onto the homogeneous white Kaolin clay surface to increase soil texture for effective PIV analysis (White et al., 2003). The perspex screen was then re-attached to complete the model. This method of installation inevitably introduced additional stresses onto the clay around the pile, and might not be truly representative of how under-reamed piles were constructed in practice (normally bored then cast in-situ). Nevertheless, it provided valuable insights into the pile-clay interaction under uplift conditions. It was also discovered that silicon grease did not provide a good seal against clay trying to squeeze into gaps between the pile and perspex during perspex reinstallation and actual pile uplift. Precautions to minimise the occurrence of this phenomenon were taken, which involved ensuring the exposed clay surface was level (non-protruding), and that the flat pile face was in complete contact with the perspex window.

In both cases it was crucial to ensure that the piles remained vertical and not inclined during and after installation. A spirit level was used to constantly monitor the verticality of the pile.

Harris (2014) and Hughes (2015) foresaw the problems of slow set-up, difficult installation of piles and limited number of tests to obtain repeat data for testing in clay compared to sand, which were proven to be realistic. However, having done tests on both soil types in this project, the notion that more apparatus was required during model preparation in clay was debatable.

3.4 Equipment

All tests were displacement-controlled, i.e. uplift of the pile was generated by applying a constant rate of upward displacement using a 1D actuator connected to the pile head. The rate of displacement was controlled by a shearbox and the actuator was driven into motion by a power supply. To maintain consistency across the entire set of tests, a low rate of 0.1mm/s was adopted such that all tests remained static and any dynamic effects were eliminated. For sand, there was sufficient time for any settlement to occur. For clay, this rate was thought to be quick enough to simulate undrained conditions.

Other experimental equipment included a GoPro HERO4 Black Edition camera and two portable filament lamps. The former recorded 4k resolution videos of all tests, which were then converted into series of still images for use in PIV analysis. The latter was necessary to maintain the quality and clarity of the recorded videos.

3.5 Instrumentation

3.5.1 Load measurement

An 800 N miniature load cell interconnected between the pile head and the actuator was employed in all tests to measure the instantaneous uplift force applied to the pile. Calibration was performed before and after each test to ensure data accuracy and consistency. The process involved threading a load hanger instead of the pile onto the load cell via a pin connector, adding known masses in increments within the expected range of applied loads and recording the corresponding output voltage (Figure 15(a)). A linear calibration curve was then constructed for the conversion from raw voltage readings into applied loads (Figure 15(b)).

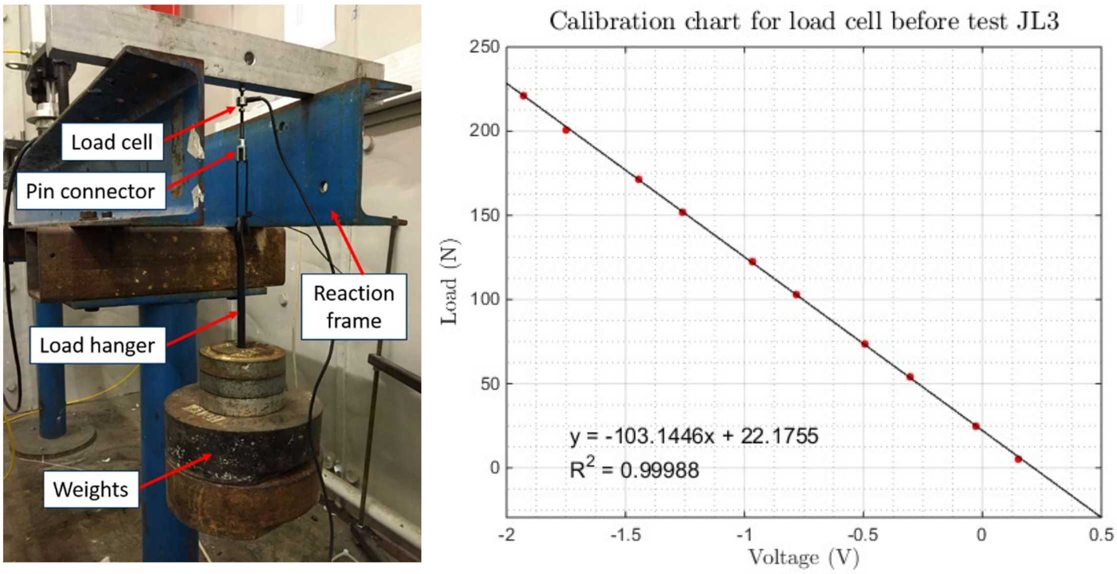

(a) (b)

Figure 15: (a) Load cell calibration set-up (b) typical load cell calibration curve

3.5.2 Displacement measurement

A linear variable differential transformer (LVDT) was employed in all tests to measure the actual pile head displacement. It was fixed at a position above the actuator carriage, so that during experiments the device could remain vertical on a flat measuring surface. Again, calibration was performed before and after each test to ensure data accuracy and consistency. The process involved imposing known displacements using a digital Vernier caliper and recording the corresponding output voltage (Figure 16(a)). A linear calibration curve was then constructed for the conversion from raw voltage readings into applied displacements (Figure 16(b)). It was observed that linearity did not hold at the extreme ends of travel for the LVDT, therefore readings from these extreme regions of the LVDT were always avoided during tests.

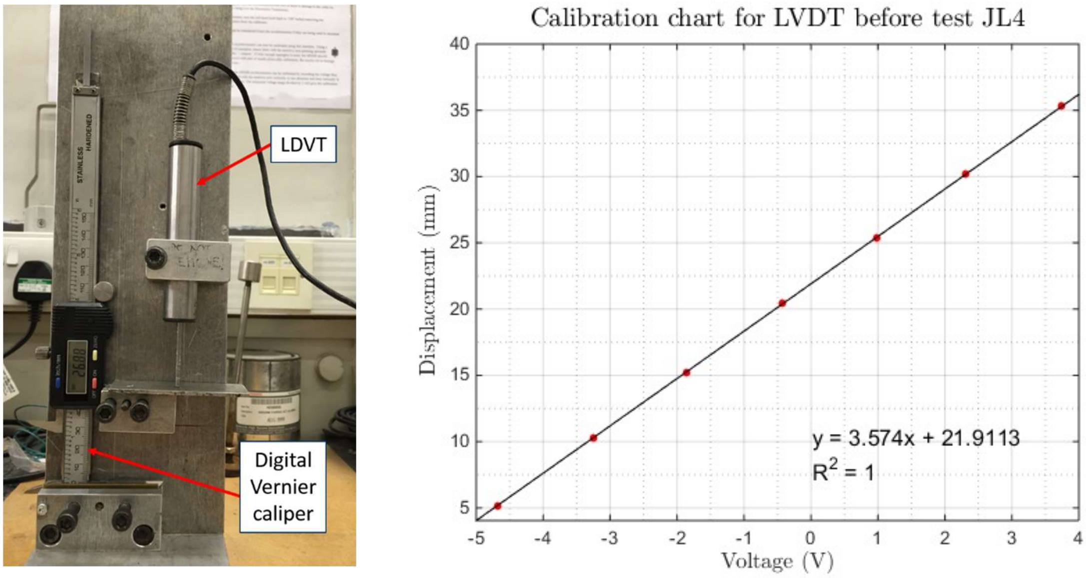

(a) (b)

Figure 16: (a) LVDT calibration set-up (b) typical LVDT calibration curve

3.5.3 Data acquisition

Data from both instruments was recorded continuously by DASYLab 9.0 data logging software for subsequent analysis.

3.6 Data processing

MATLAB R2014b was used to analyse the obtained load-displacement data. PIV analysis was also undertaken in MATLAB using both the original GeoPIV software developed by White & Take (2002) and the latest version GeoPIV-RG (Stainer et al., 2015). The selected patch size was 50 x 50 pixels at a 50 pixel spacing. Under this patch size, all soils were successfully tracked and results were produced with satisfactory resolutions. Attempts on finer patches had led to considerably more wild vectors, thus they were not preferred. In light of the large amount of extracted still frames (due to long video lengths ≈ 20 minutes) and enormous video file size for some tests (> 8 GB), balance had to be maintained for the trade-off between computational effort and resolution.

3.7 *Full experimental set-up*

The complete experimental set-up for the tests is shown in Figure 17.

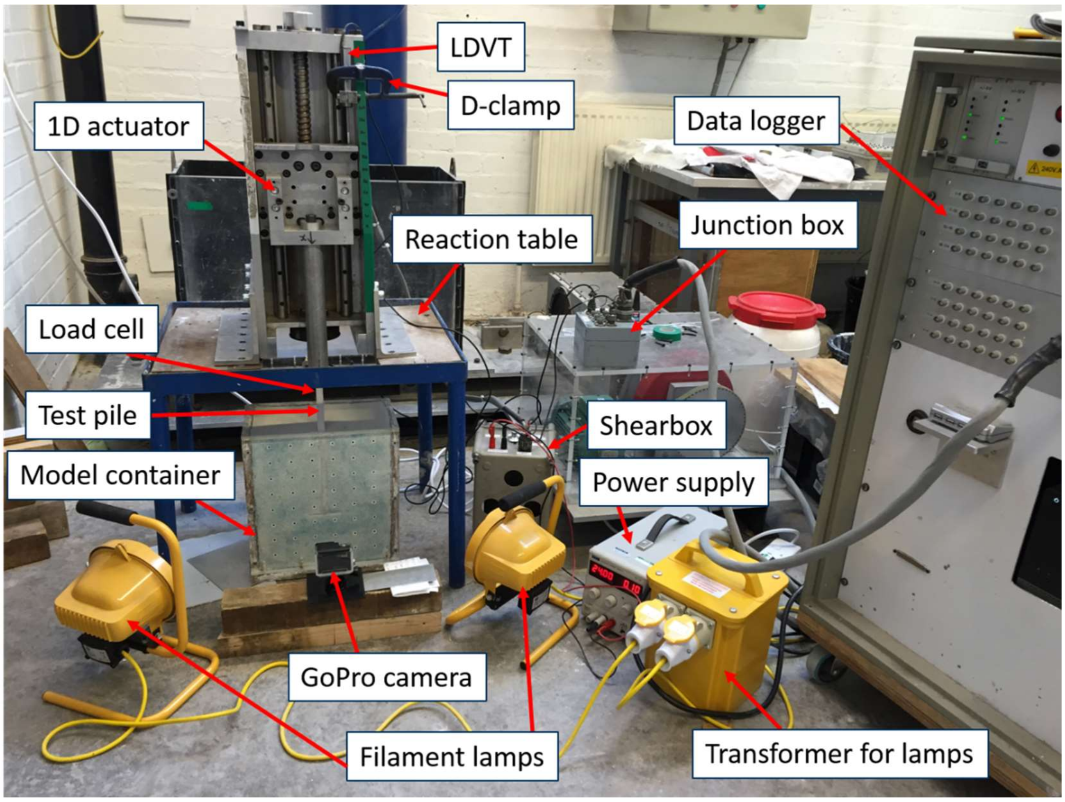

Figure 17: Experimental set-up

Considering the relatively small and light box used in the current project, there were concerns of the entire box being lifted up along with the pile and soil it contained. This was resolved by wedging in some timber pieces above the box and under the table (not shown in the above figure). Reaction from the table plus the substantial weight of the actuator successfully prevented box uplift without compromising the lighting conditions on the model display surface for PIV analysis.

3.8 *Experimental procedure*

Test in sand was performed according to the following procedure:

1. Fix the half space model pile onto the perspex screen using a D-clamp and mask tape. Ensure the verticality of the pile by using a spirit level.
2. Pour sand into the container in layers of 35 mm thick using the manual sand pourer, noting the amount of sand added. For every layer, pour an approximately 3 mm thick stream of blue sand up against the perspex window. Remove the mask tape sequentially as sand

gradually fills up the container. Level the sand surface once the desired depth is reached. Remove the D-clamp subsequently.

3. Connect the load cell onto the pile head. Position the 1D actuator and connect it to the other end of the load cell. Attach the LVDT onto the actuator carriage. Check all equipment to ensure it is functioning properly.
4. Set the shearbox and power supply to the correct settings. Start recording of the camera and data logger at roughly the same time. Activate the actuator. Record data until post-failure. Detach all instruments from the model afterwards.
5. Remove soil and clean the container to prepare for the next test.

Tests in clay were performed according to the following procedure:

1. Detach the perspex window. Cut the clay block to a volume similar to that of the box. Fit the block into the open-faced box and minimise any gaps between the clay and the container. Slice off any clay protruding from the exposed face.
2. Push the pile into the clay with the flat side facing upwards at the required position until it is levelled with the surrounding clay. Ensure the verticality of the pile by using a spirit level. Sprinkle blue sand onto the clay surface. Re-attach the perspex screen. Weigh and note the mass of the completed model.
3. Follow steps 3 to 4 for testing in sand.
4. Conduct hand vane shear test in undisturbed regions of the clay.
5. Follow step 5 for testing in sand.

3.9 Test schedule

The overall test schedule is presented in Table 2. The embedment depth was kept constant throughout at D = 180 mm, giving an embedment ratio of $\frac{D}{B}$ = 3.0 for all tests.

The first test in sand (test JL1) had two purposes. It served as a precursor allowing familiarisation of the general experimental flow and procedure in preparation for future tests and enabled comparisons between sand and clay to be made. Subsequent clay tests (tests JL2 to JL5) on the contrary were highly dependent on the supply of clay from the laboratory.

Table 2: Project test schedule

Test Name	Aim	Soil Type	Soil Properties	Under-Ream Angle [°]
JL1	To determine the load-displacement and failure mechanism characteristics of a 45° under-reamed pile in dense sand	Hostun HN31 Sand	'Dense' $I_D \approx 70\%$ $\gamma \approx 15.36$ kN/m^3	45
JL2	To determine the load-displacement and failure mechanism characteristics of a plate anchor in soft clay	Kaolin Clay	'Soft' $c_u \approx 10.45$ kPa $\gamma \approx 15.81$ kN/m^3	0
JL3	To determine the load-displacement and failure mechanism characteristics of a 45° under-reamed pile in soft clay	Kaolin Clay	'Soft' $c_u \approx 12.81$ kPa $\gamma \approx 16.12$ kN/m^3	45
JL4	To determine the load-displacement and failure mechanism characteristics of a plate anchor in stiff clay	Kaolin Clay	'Stiff' $c_u \approx 15.53$ kPa $\gamma \approx 15.79$ kN/m^3	0
JL5	To determine the load-displacement and failure mechanism characteristics of a 45° under-reamed pile in stiff clay	Kaolin Clay	'Stiff' $c_u \approx 19.00$ kPa $\gamma \approx 16.78$ kN/m^3	45

3.10 Experimental accuracy

Main sources of experimental error included:

- Orientation of the model piles and the load cell – the latter was very sensitive to any unintended moment applied on it. Measures described in section 3.3.2 were taken to ensure the verticality of components so that the transmitted load was purely axial. The components were aligned precisely before assembling with due care.
- Assumption of perfectly smooth piles – although the uplift capacity of under-reamed piles may be dominated by end-bearing of the enlarged base (Chaudhuri & Symons, 1986; Poulos & Davis, 1980), shaft friction may still exist and contribute partly towards the capacity. Various methods to evaluate the shaft resistance may be used based on 'effective pile lengths', allowing for non-contributing regions near the enlarged base. Refer to section 6.1.
- Hand vane shear test – accuracy of which is questionable since a fair range of c_u values was obtained for the same clay sample using vanes of different sizes.

4. Pile Load-Displacement Response

4.1 Experimental results

The set of non-dimensionalised load-displacement curves obtained from the tests are presented in Figure 18, showing the relationship between normalised uplift capacity $N_{qu} = \frac{Q_u}{\gamma AD}$ and normalised displacement $\frac{\delta}{B}$.

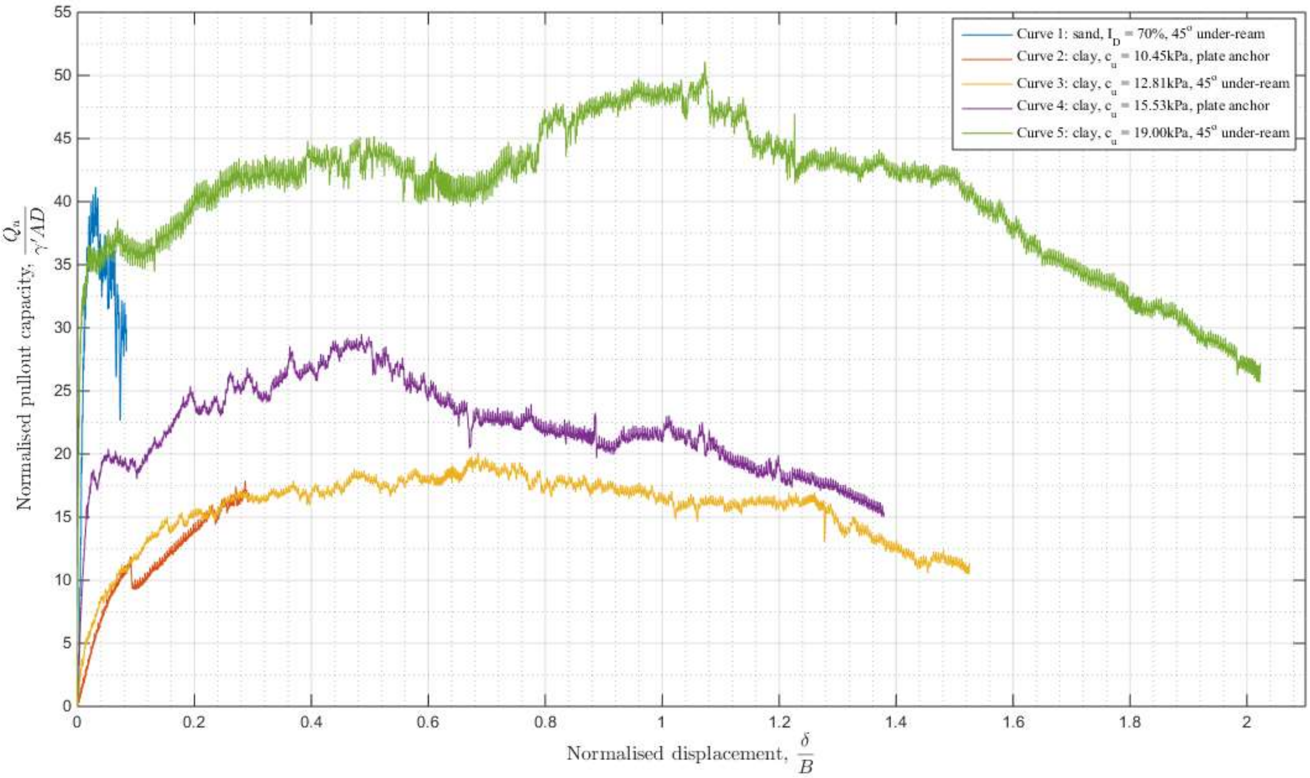

Figure 18: Non-dimensionalised load-displacement curves derived from tests

Curve 1 displays results obtained from test JL1, in which the 45° under-reamed pile was embedded in homogeneous dense sand. The form of this curve (a better view of which can be found in Figure 21) resembles the expected behaviour of dense sand upon direct shearing whereby the sand initially dilates, reaches a well-defined peak strength at a relatively small displacement, then softens post-peak towards a critical state. Fluctuations in load at large displacements (relative to the load-displacement profile of the sand) are observed around normalised displacements of $\frac{\delta}{B} \approx 0.07$.

Curves 2 to 5 indicate data gathered from tests JL2 to JL5 respectively, representing all possible permutations for the given pile types (plate anchor or 45° under-reamed pile) and soil properties (soft or stiff clay). Within the given data ranges, all four curves have similar forms scaled differently along both axes of the graph. Several regimes of the pile behaviour in clay can be identified from the curves, and they are summarised in Table 3. This classification will also be used to aid the subsequent analysis of PIV results detailed in chapter 5.

Table 3: Different regimes of load-displacement behaviour of under-reamed piles embedded in clay

Regime	Description
1	Increase in capacity at small displacements with initial stiffness
2	Gradual increase in capacity towards peak mobilising large displacements, i.e. yielding
3	Attainment of peak capacity, i.e. ultimate state
4	Slight softening towards a temporary plateau
5	Strain softening (falling branch) at very large displacements

It is to be explained here that the 'incomplete' curve 2 was due to test JL2 being the first test in clay in this project, the imposed displacement was discovered after the test to be insufficient in causing failure of the clay. In other words, the displacement to failure for clays was underestimated. As a result, the subsequent tests were conducted up to very large displacements ($\frac{\delta}{B}$ > 1.3) in order to obtain a more comprehensive picture of the pile response in clay. Nevertheless, a close examination on curve 2 reveals some important features of under-reamed piles embedded in clay (see section 5.1.1).

4.1.1 Comparison between soft and stiff clays

This section focuses on comparing among curves 2 to 5 only. Figure 18 shows that in regime 1, the initial stiffness of the piles in stiff clay is much greater than that in soft clay, as logically expected. For stiff clays the initial response appears to be linear up to a normalised displacement of $\frac{\delta}{B} \approx 0.02$, while for soft clays the stiffness degrades incrementally as soon as displacement is imposed. The different magnitudes of initial stiffness for the curves suggest some correlation with clay strength (c_u), which can be described by a power law as illustrated in Figure 19.

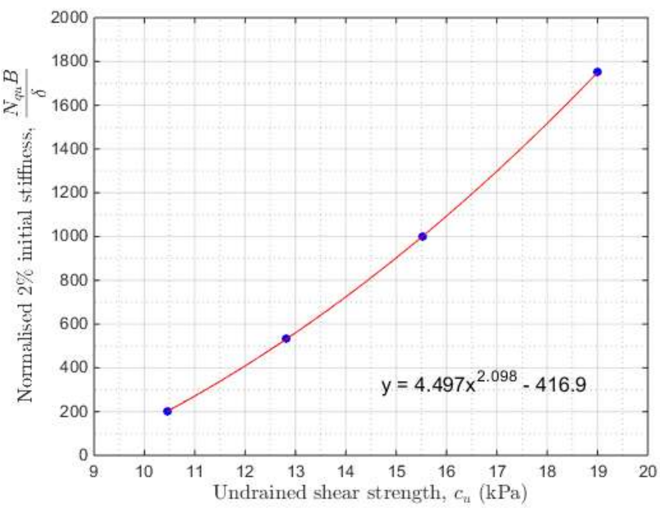

Figure 19: Relationship between initial stiffness and undrained shear strength

Consider regime 3 at the ultimate state. In light of the vertical scaling of the different curves the results strongly suggest a peak capacity trend with clay strength despite the pile in test JL2 did not reach its maximum capacity. Another power law can be used to describe this trend (Figure 20). Further verification is warranted as only three data points were available in the present study. However, it is intuitive to suggest that the ultimate capacity is greater for stiff clays with a higher c_u than soft clays with a lower c_u. On the other hand, there are no obvious relations regarding the displacement to failure for the different clay samples tested.

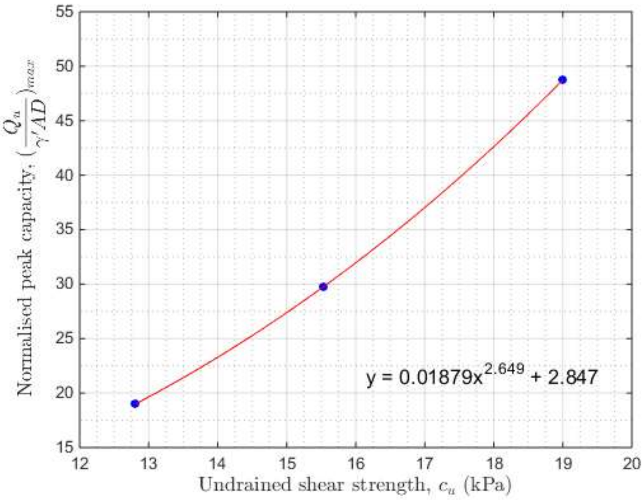

Figure 20: Relationship between peak capacity and undrained shear strength

In regime 4, the results indicate a steeper post-peak reduction of capacity onto a plateau in stiff clays than in soft clays. Possible explanation for this based on the underlying failure mechanism is given in section 5.2.2. Again this may require further verification as regime 4 had not been reached during test JL2.

No apparent trends are observed in regimes 2 and 5. The steepness of the falling branch in regime 5 appears to be similar across the different tests, while its span is solely dependent on the time at which the tests ended (arbitrarily chosen).

4.1.2 Comparison between under-ream angles

In this section, curves 2 and 4 for the plate anchor are compared to curves 3 and 5 for the 45° under-reamed pile, both embedded in clay. The main difference in the curves due to a change in under-ream angle (between 0° and 45°) is the presence of a sudden dip in load within regime 2 observable for the plate anchor but less apparent or non-existent for the 45° under-reamed pile. This is more clearly seen by zooming in the initial portions of the curves up to a normalised displacement of say $\frac{\delta}{B} \approx 0.3$ (Figure 21). The sudden dips in load for the plate anchor are highlighted and labelled on the figure as 'A' and 'B' for soft and stiff clays respectively. The occurrence of these dips is best explained with regards to the problem geometry and failure mechanism. See sections 5.1.1, 5.1.2 and 5.2.1.

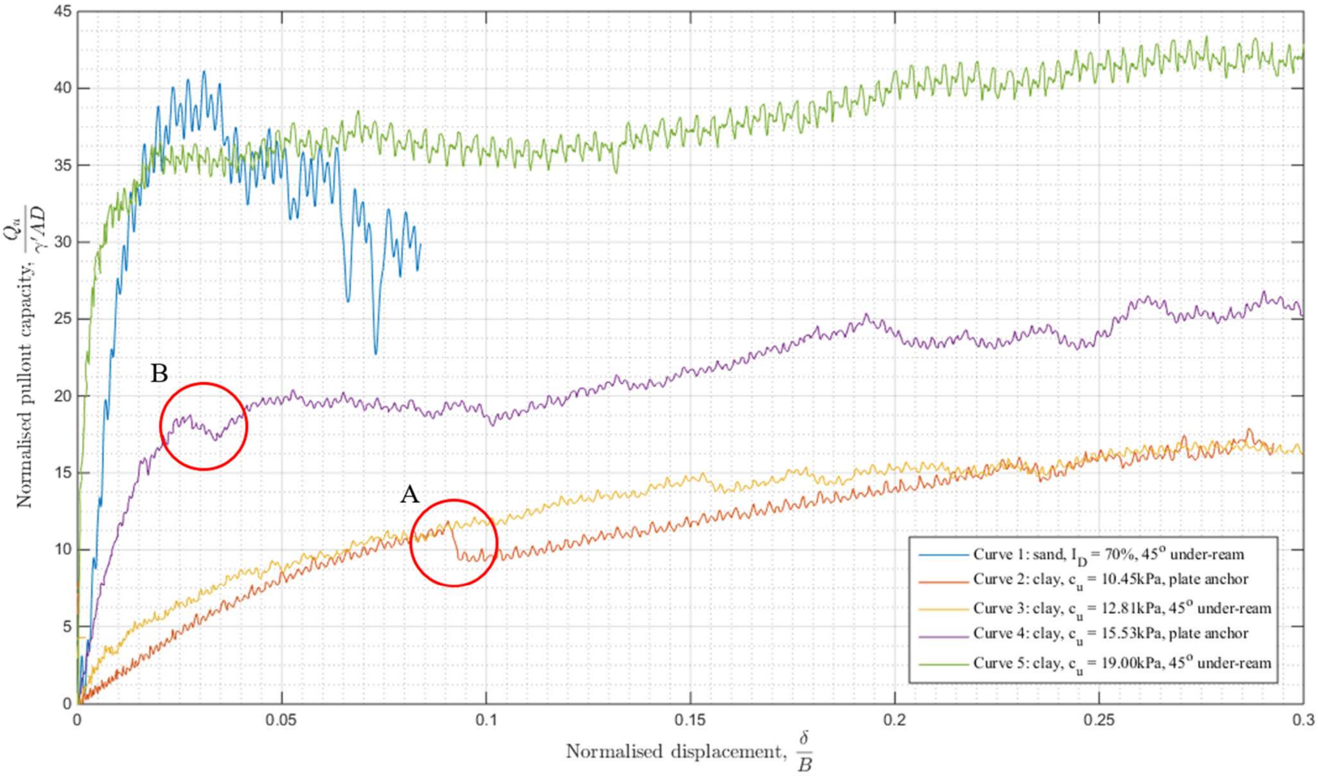

Figure 21: Close-up of the non-dimensionalised load-displacement curves up to a normalised displacement of 0.3

4.1.3 Comparison between sand and clay

In this section, curves 2 to 5 are compared against curve 1 to contrast the pile behaviour in clay and in sand. Initial stiffness of the 45° under-reamed pile in stiff clay (curve 5) is comparable to that in dense sand (curve 1), both showing initially stiff behaviour at small displacements ($\frac{\delta}{B}$ < 0.02). However, three key differences between pile behaviour in sand and clay are observed from the results:

1. Clays mobilise significantly larger displacements to failure than sands and exhibit a high degree of plasticity, as expected for soft cohesive soils compared to non-cohesive granular soils.

2. For the stiffest clay (curve 5), the normalised peak capacity attained was higher than that for the dense sand (curve 1), which is regarded as counter-intuitive. This is because the stiffest clay used in this project was still very 'soft' compared to typical values of c_u for Kaolin clay encountered in practice, and the sand was a dense frictional material which should in theory possess higher strengths. Two possible explanations for this – firstly, the

sand in reality might not be as dense as having a relative density I_D = 70% due to heterogeneities (e.g. local regions of loose sand) present within the stratum, introduced during the process of manual sand pouring. Secondly, the reliability of hand vane shear test to determine a representative value of c_u for clay is dubious, as explained in section 3.10. Hence, it is recommended to treat the c_u values determined in this project as indicators of 'relative degrees of strength' among the samples, rather than associating the absolute values to any expected soil properties.

3. Post-failure instability of sand is analogous to strain softening of clay in that they both take place at large displacements, but the underlying physical phenomena of the two are distinctively different (see sections 4.2.3 and 4.2.4).

4.2 Comparison to literature

4.2.1 Load-displacement curve form

The observed load-displacement behaviour of the 45° under-reamed pile in dense sand (curve 1) is found to be in alignment with previous similar research (Dickin & Leung, 1990; Hopkins, 2012; Harris & Madabhushi, 2014; Hughes, 2015), in that the curve form mimics the expected behaviour of dense sand subjected to simple shear (as described in section 4.1). This curve form is also similar to that proposed by Ilamparuthi et al. (2002) for shallow circular plate anchors in dense sand with an embedment ratio of $\frac{D}{B} = 3$ (Figure 22). However, Harris (2014) and Hughes (2015) obtained contradicting results in which for a fixed embedment the shape of the curves varied depending on sand density. Ilamparuthi et al. (2002) on the other hand presented curves that were dependent only on embedment but not density, which seemed to violate the expected behaviour of sand being sheared. Despite of this disagreement in literature, the uplift behaviour of plate anchors in dense sand is beyond the focus of this project since only the 45° under-reamed pile was tested in dense sand.

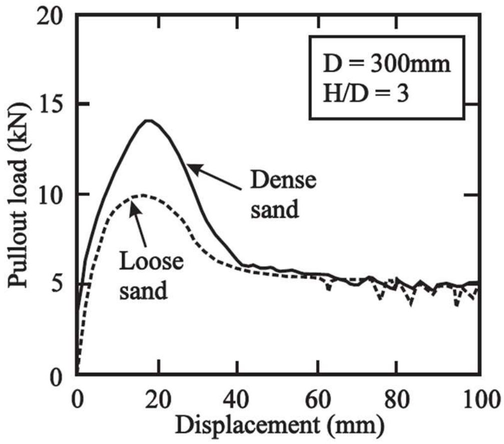

Figure 22: Load-displacement relationship for shallow circular plate anchors in sand (Ilamparuthi et al., 2002)

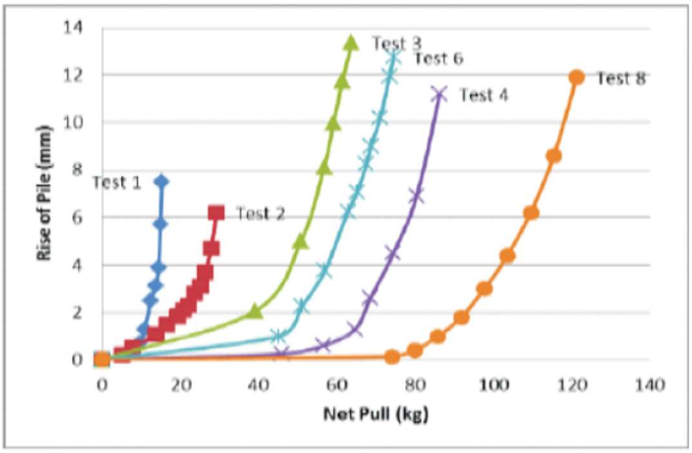

Figure 23: Load-displacement curves observed from some model under-reamed pile tests in soft clay (Golait et al., 2014)

In clay, the overall shape of curves 2 to 5 is in general agreement with most experimental and numerical results on uplift of plate anchors (Chaudhuri & Symons, 1986; Rattley et al., 2008; Singh & Ramaswamy, 2008) and of under-reamed piles (Sakajo et al., 1995; Chai et al., 2005; Lehane et al., 2008; Xu et al., 2012; Golait et al., 2014) reported in literature. In most cases there was substantial yielding followed by gradual approach towards a maximum in capacity mobilising relatively large displacements (regimes 1 and 2). The peak capacity in regime 3, however, might or might not have attained subsequently (Figure 23). On the contrary, most researchers presented a plateau region maintained at the peak load level beyond the ultimate state (i.e. perfectly plastic stage), instead of a slight reduction in capacity towards a later temporary plateau region characterised as regime 4 in this project. This may be explained with the aid of the underlying failure mechanism, as described in section 5.2.5. More apparently, the post-failure strain softening behaviour at very large displacements (falling branch in regime 5) in the present project was not captured by most researchers apart from Chai et al. (2005). More details on this in section 4.2.3. Overall speaking, softening behaviour of clays had not been depicted in general by the majority of previous researchers.

4.2.2 Ultimate uplift resistance

The ultimate uplift resistance of 45° under-reamed pile in sand and the corresponding displacement to failure (results from test JL1) of this project are compared to those of other researchers carrying out similar experimental work in under-reamed piles. This is presented in Table 4. Percentage errors are derived relative to current test results.

It is worth noting that in the present test the load-displacement plot was obtained using half-space piles rather than full 3D model piles. Since the projected base area A was halved, the normalised peak capacity $N_{qu} = \frac{Q_u}{\gamma AD}$ should be expected to halve if full 3D model piles were to be used in this test instead. Hence, the value of N_{qu} quoted in Table 4 has been corrected for the half models. In light of this, Table 4 shows good agreement between current test results and those gathered by Hughes (2015), less so compared to results reported by Harris & Madabhushi (2015) and Hopkins (2012). This is thought to be due to the sand density attained by the former (I_D = 75%) being higher that achieved by the latter (I_D = 60% and 48.4%).

Table 4: Comparison of ultimate uplift capacity and displacement to failure for tests in dense sand

Reference	**Test Description**	**B [m]**	**N_{qu} [-]**	**$\left(\frac{\delta}{B}\right)_{fail}$ [-]**	**% error in N_{qu}**	**% error in $\left(\frac{\delta}{B}\right)_{fail}$**
Current test	1g half space model test on 45° under-reamed pile in dense sand	0.06	20	0.03	-	-
Hughes (2015)	1g 3D model test on 45° under-reamed pile in dense sand	0.06	21	0.01	+5.0%	-66.7%
Harris & Madabhushi (2015)	1g 3D model test on 45° under-reamed pile in dense sand	0.06	13	0.01	-35.0%	-66.7%
Hopkins (2012)	1g 3D model test on 45° under-reamed pile in dense sand	0.06	16	0.008	-20.0%	-73.3%
Dickin & Leung (1990)	Centrifuge model test on 45° belled piers in dense sand	1	7.5	0.06	-62.5%	+100%
Tucker (1987)	Full-scale field test on 45° belled piers in dense sand	1.2	6.3	0.02	-68.5%	-33.3%

Results of centrifuge tests conducted by Dickin & Leung (1990) contrast the results of 1g model tests significantly, by showing a much lower normalised ultimate capacity at a much greater failure displacement (i.e. pile response was less stiff). The cause of which is believed to be scale effects, as Dickin & Leung (1990) used bigger model piers close to field size. Once again it can be emphasised that small scale 1g model tests should not be used to predict behaviour of fully sized piles. Similar argument can be applied to the results obtained by Tucker (1987), who conducted field tests with fully sized piers of base diameter that was 20 times greater than that used in the present study. Also, soil properties and characteristics tend to be highly variable and less controlled in the field.

For clays, comparing the relative magnitudes of normalised ultimate capacity from this project and from other investigators is found to have limited value because of the boundless dissimilarities, variability and uncertainties inherent in the specifics across different tests (e.g.

significantly different clay types, unknown stress histories, completely different methods of clay preparation and uplift testing, rate and scale effects, not using non-dimensionalised parameters where necessary etc.). Nevertheless, various researchers have postulated generalised methods to estimate the ultimate uplift capacity of under-reamed foundations embedded in clay. Several of these suggested methods of calculation are discussed and compared against results obtained from the current project in chapter 6.

4.2.3 Post-failure strain softening of clay

Most results from literature for clays exhibited elasto-plastic behaviour, with the plastic part being almost perfectly plastic, omitting what is considered as regime 5 in the present study. As explained previously in section 4.2.1, one group among the few researchers who considered strain softening behaviour of clays when under-reamed piles were subjected to uplift was Chai et al. (2005), who attempted to provide explanations for the inadequacy of research in this phenomenon (and thus why this strain softening behaviour was not captured in many published results) despite the fairly widespread study on uplift capacity of foundations embedded in clay. This could be attributed to either the difficulty in monitoring stress-strain behaviour of every single soil element within the model during testing, or the limited capability of many elasto-plastic constitutive models used in numerical studies to simulate strain softening behaviour.

In addition to the reasons suggested by Chai et al. (2005), another possible explanation is thought to be due to the nature of different tests being carried out – whether they were displacement-controlled or load-controlled. For displacement-controlled tests (as in the current project), it is believed that many investigators simply did not continue their tests beyond the plateau region to realise the existence of a falling branch (softening) at very large displacements (Figure 24), which might happen for example when the experimental apparatus had reached its limits in imposing upward displacements, hence giving the impression that there was no apparent peak

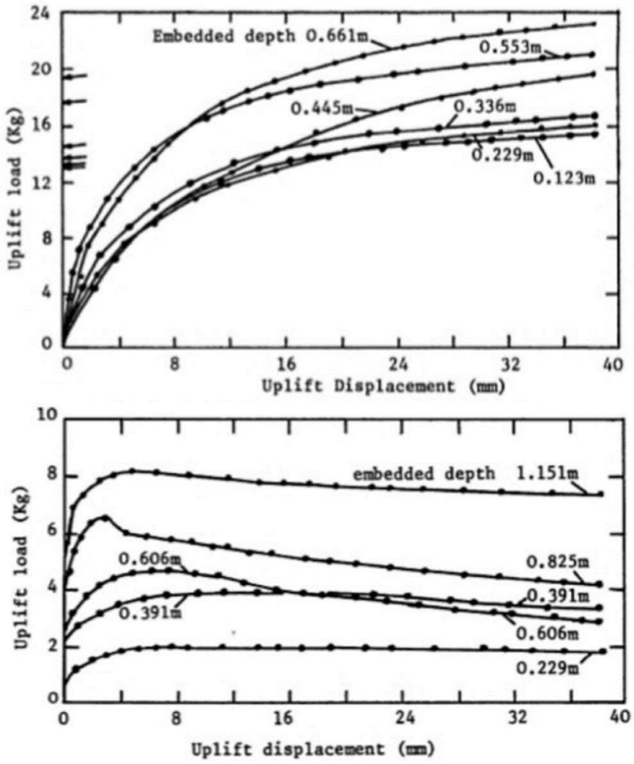

Figure 24: Load-displacement curves for model enlarged base piles (above) and straight shafted piles (below) in clay (Chaudhuri & Symons, 1986)

capacity for the under-reamed piles tested (Chaudhuri & Symons, 1986). This was in contrast to the results obtained in the present study. Yet for normal straight shafted piles this softening behaviour was found to be more gradual and initiating at much smaller displacements (Figure 24), thus was successfully captured in various results. For load-controlled tests, stress states characterised by softening were simply impossible to reach if the load was applied say incrementally by adding weights onto a hanger over a lever system (Figure 25). Differences between these two types of tests were found to have some important implications on the pile load-displacement response (see section 5.1.1).

It is to be noted that, however, the physical nature behind the softening behaviour observed in the current tests and results from Chai et al. (2005) is in fact quite different. The latter involved an artificial enforcement of strain softening characteristics for the model soil in numerical analyses, while the former was associated with a physical reasoning as detailed in section 5.2.2.

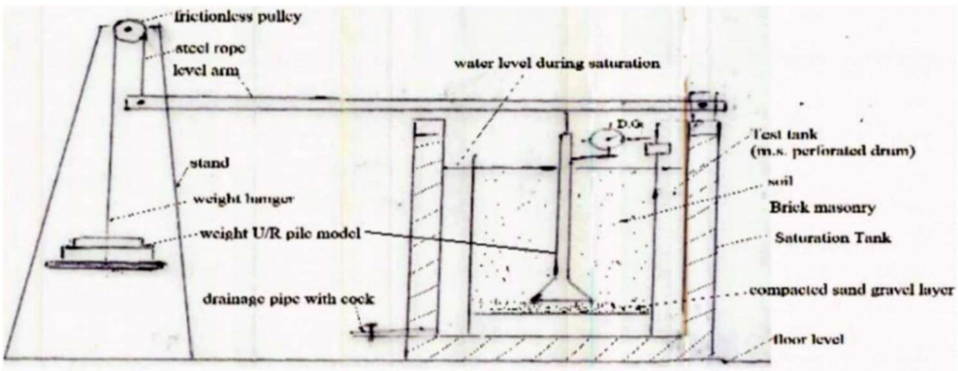

Figure 25: Example experimental set-up for a load-controlled pullout test (Golait et al, 2014)

4.2.4 Post-failure arching and instability of sand

As mentioned before in section 4.1, oscillations in load at large displacements post-peak are observed for the 45° under-reamed pile in sand (curve 1). This was caused by the phenomenon of soil arching in sand (Ilamparuthi et al., 2002), whereby sand surrounding the pile base formed an arch utilising resistance as the pile moved up, but the local soil packing became unstable due to the large cavity under the pile base. Consequently, the arch collapsed to fill up the void, causing the load to decrease. A new soil arch was then formed as the pile rose further. The cycle then started over again and repeated itself, leading to load fluctuations. This post-failure instability was also observed for under-reamed piles by Dickin & Leung (1992), Harris & Madabhushi (2015) and Hughes (2015). In particular, Harris & Madabhushi (2015) postulated that the displacement marking the start of this instable behaviour was independent of sand density. Additional tests on sands with a range of relative densities will have to be performed in order to validate this.

5. Soil Failure Mechanism Characterisation

In this chapter, results from PIV analyses are presented, described and compared. Wherever possible, for the mechanism represented by each test, progressive vector plots superposed on the respective starting image showing the small strain, peak and post-peak failure mechanisms are given. The vectors shown were scaled up appropriately for clarity. In general, the small strain failure mechanism refers to the initial part of the tests where small displacements were imposed. The peak failure mechanism corresponds to the attainment of maximum capacity. The post-peak failure mechanism indicates the closing part of the tests beyond the ultimate state where large displacements had been applied. Each set of results is further complemented by a cumulative vector plot in object space which displays the overall displacement field from start to end of the test. During the process of PIV analysis, wild vectors due to tracking failures were removed manually.

5.1 Plate anchor

5.1.1 Soft clay mechanism

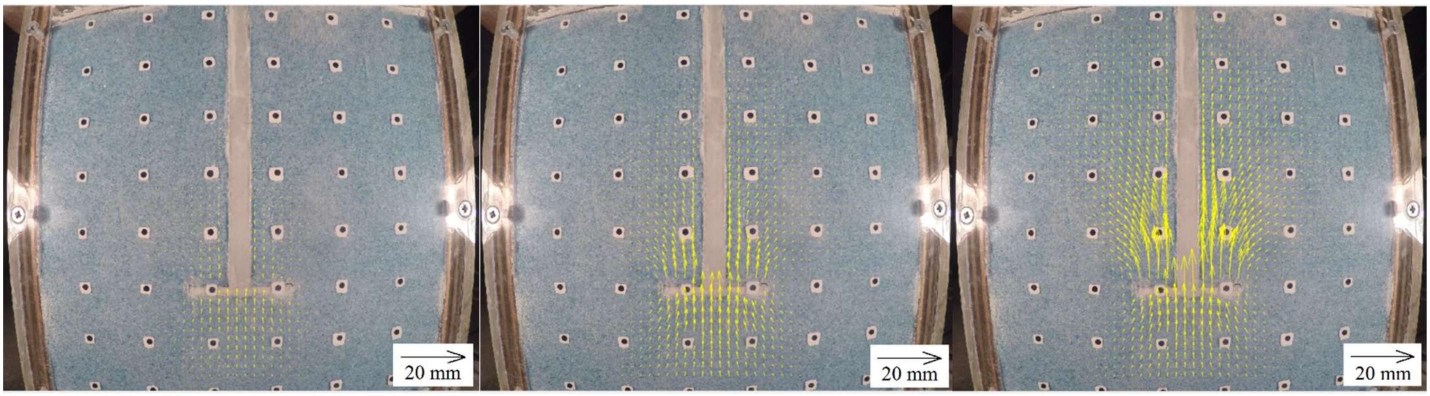

(a) (b) (c)

Figure 26: Progressive PIV vector plots for plate anchor in soft clay
(a) Small strain, $\frac{\delta}{B} \approx 0.01$; (b) Pre-peak, $\frac{\delta}{B} \approx 0.10$; (c) Pre-peak, $\frac{\delta}{B} \approx 0.29$

It is worth reminding that for this test (test JL2), the soil only experienced a small degree of yielding and the peak capacity had not been reached. Refer to section 4.1 for details. Nevertheless, some remarkable characteristics of clay behaviour under uplift loading can be inferred from Figure 26. At small strains (regime 1), a confined region of soil around the enlarged base was mobilised in the form of a bulb (Figure 26(a)). Since the soil outside the bulb was not moving, it implies that the soil above the plate surface was being compressed, while soil below the plate base was being sucked up. This is perhaps logically expected for cohesive soils. As the imposed displacement increased (regime 2), the bulb grew larger in size, involving greater compression and suction at top and bottom of the plate respectively (Figure 26(b)). It can be inferred from Figure 26(b) and (c) that the base suction was lost at a normalised displacement of $\frac{\delta}{B} \approx 0.10$, because the vectors below the pile base remained unchanged starting from that displacement onwards. On the other hand, more and more soil above the plate experienced compression as the upper part of the bulb increased its extent both vertically and laterally (Figure 26(c)).

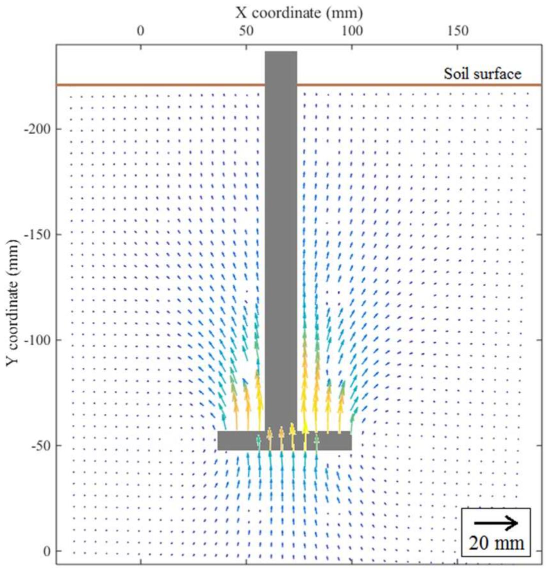

Figure 27: Cumulative PIV vector plot for plate anchor in soft clay

The suction behaviour of clay under the pile base (Figure 28) was discovered to have a significant effect on the load-displacement response of the pile. Referring back to Figure 21 in section 4.1.2, the sudden dips in load can now be explained by this phenomenon. When $\frac{\delta}{B} \approx 0.10$, the dip marked 'A' on Figure 21 corresponds exactly to the instant when the base suction was lost (i.e. the breakaway state). Analysis of curve 2 showed that the pile was unloaded by about 22% all of a sudden due to the loss of base tension, and the stiffness degraded by about 44% accordingly. If this test were to be conducted load-controlled, dip A would not be captured. Instead, a dynamic jump in pile displacement of at least 50% (from $\frac{\delta}{B} \approx 0.10$ to 0.15) would occur. This may pose serious issues on the SLS performance of such foundations used in practice, where loading is typically applied in a load-controlled manner. The proof of this taking into account scale effects is beyond the scope of this project.


Figure 28: Evidence of base suction

5.1.2 Stiff clay mechanism

The small strain (regime 1) failure mechanism is found to be similar to that of soft clay, where resistance was mobilised in a localised bulb (Figure 29(a)). By comparing dips A and B in Figure 21, it appears that the base suction was slightly less in this case than in soft clay (dip B had a smaller drop in load than dip A), and breakaway occurred at an earlier stage (dip B occurred at a lower displacement than dip A). The latter observation is perhaps intuitive for the

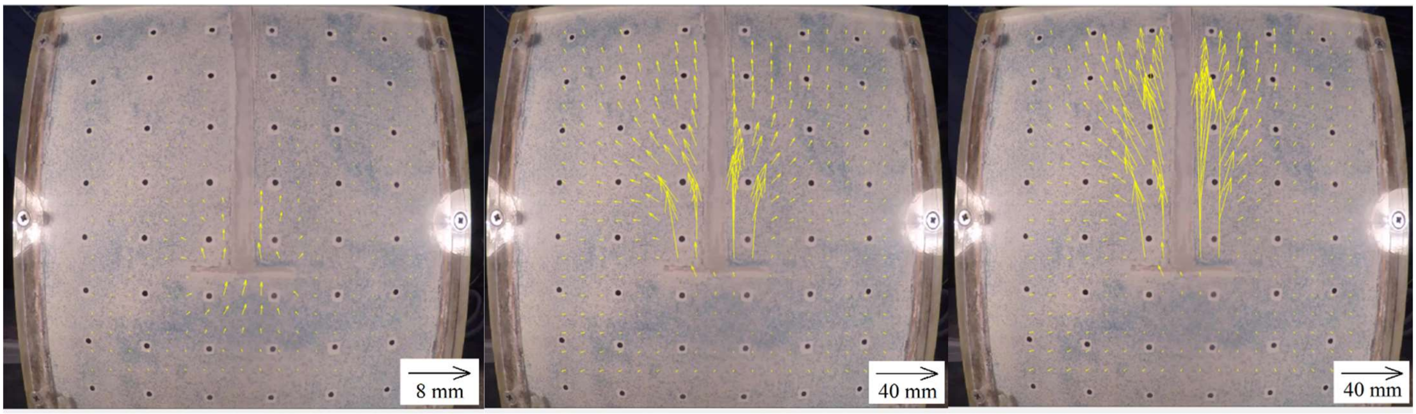

(a) (b) (c)

Figure 29: Progressive PIV vector plots for plate anchor in stiff clay
(a) Small strain, $\frac{\delta}{B} \approx 0.01$; (b) Peak, $\frac{\delta}{B} \approx 0.48$; (c) Post-peak, $\frac{\delta}{B} \approx 1.36$

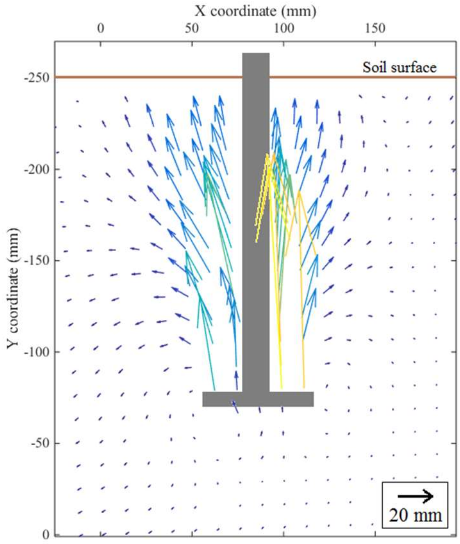

Figure 30: Cumulative PIV vector plot for plate anchor in stiff clay

stiffer behaviour in this case. Approaching the peak response at large imposed displacements (regime 3), significant compression in the soil closely above the plate was observed, while soil next to the plate edges was being squeezed sideways (Figure 29(b)). There was a tendency for vectors above the compression zone to rotate towards the vertical with decreasing depth, giving a bowl (or convex cone) shape to the overall plastic zone above the plate. The post-peak mechanism (regime 5) amplified the peak response and brought the mechanism up to the ground surface, causing the surface around the pile shaft to heave.

5.1.3 Comparison to literature

The mobilisation zone confined in a bulb observed at small displacements falls into the category of 'deep anchor, joined to soil beneath' suggested by Thorne et al. (2004), in which localised plastic flow around the plate prevailed and embedment had little effect (Figure 6(d)). On the contrary, a discrepancy was observed for the post-peak failure mechanism at large displacements – the bowl/convex conical shape obtained as opposed to the cylindrical 'shallow anchor, separated from beneath' (Figure 6(a)) proposed by Thorne et al. (2004). This was due to the fact that in the current test the pile was not embedded at a shallow depth to start with. Soil close to the pile shaft above the plate would have been displaced laterally as the pile gradually rose.

The phenomenon of base suction was also realised and observed by Meyerhof & Adams (1968) and Vesic (1971) in their model tests on plate anchors in clay. Instead of attempting to correct the results for suction as done by Meyerhof & Adams (1968), the phenomenon was considered a special feature of interest in this project, despite incomplete knowledge of clay properties and stress histories that contributed to the uncertainty in the size of this suction force (Merifield et al., 2003). Suction recorded in the present tests was partial, i.e. somewhere between 'immediate breakaway' and 'no breakaway' (Rowe and Davis, 1982), as predicted by Merifield et al. (2003). It is believed that this suction was dependent on pile installation method – whether the pile was pushed into the clay (as in this project) or placed into a cavity (of shape similar to the pile) cut out from the clay.

Upon visual inspection, tension cracks were observed to initiate only after reaching peak capacity (regime 3) with a large displacement. These cracks were situated mainly above the side edges of the plate, which extended with increasing incline to the vertical towards the soil surface to form a concave conical wedge thereafter (regime 4). The formation of these cracks were well noted by Meyerhof & Adams (1968) and Sutherland (1988). In the present study, these cracks were found to be more apparent in stiff than soft clay. The overall failure mechanism was in good agreement to that of a plate anchor with an intermediate embedment ratio of $\frac{D}{B} = 3$ observed by Sutherland (1988), in which both a local plastic zone and surface tension cracks were found to coexist.

5.2 Under-reamed pile (45°)

5.2.1 Soft clay mechanism

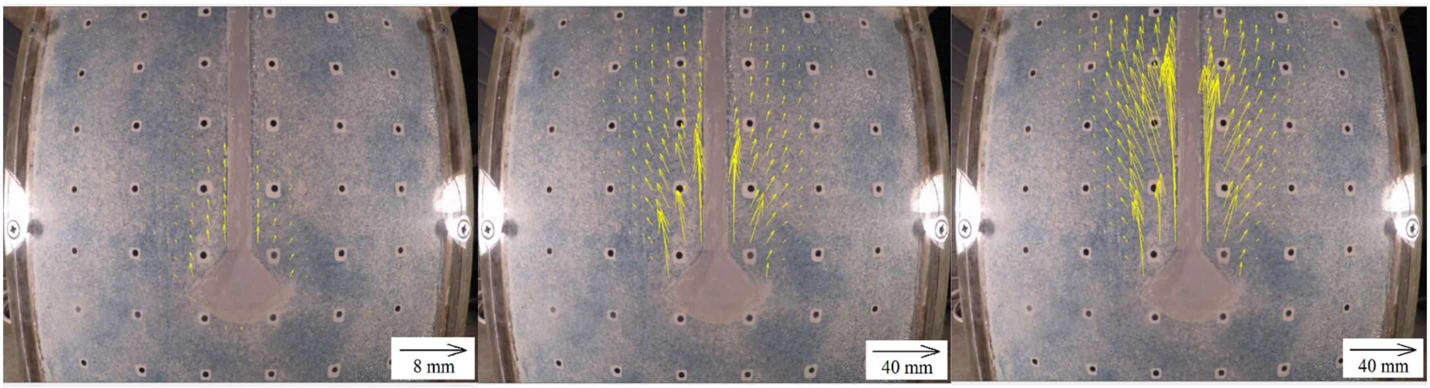

(a) (b) (c)

Figure 31: Progressive PIV vector plots for 45° under-reamed pile in soft clay
(a) Small strain, $\frac{\delta}{B} \approx 0.01$; (b) Peak, $\frac{\delta}{B} \approx 0.68$; (c) Post-peak, $\frac{\delta}{B} \approx 1.52$

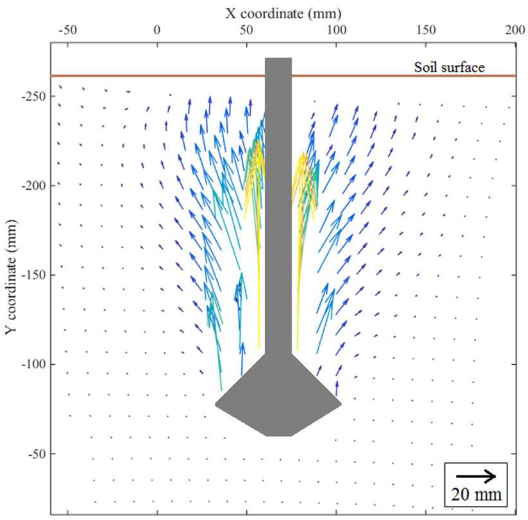

Figure 32: Cumulative PIV vector plot for 45° under-reamed pile in soft clay

The overall failure mechanism at different stages of this test was very similar to the case of a plate anchor. Description provided in section 5.1 in general also applies here. One major difference between the 45° under-ream pile and plate anchor was the relative contribution of base suction towards the ultimate capacity. For the former, considerably less suction relative to the resistance mobilised above the enlarged base was registered. This was thought to be due to the difference in geometry of the enlargement bottom surface. The flat bottom surface of the plate anchor allowed more suction to be sustained for a given projected base area, but unloading would occur abruptly during breakaway. On the other hand, the baseline profile of under-reamed piles permitted a smooth breakaway by a gradual relieve of tensile stresses, hence explaining the dips in load appeared in curves 2 and 4 but not in curves 3 and 5 (Figure 21).

5.2.2 Stiff clay mechanism

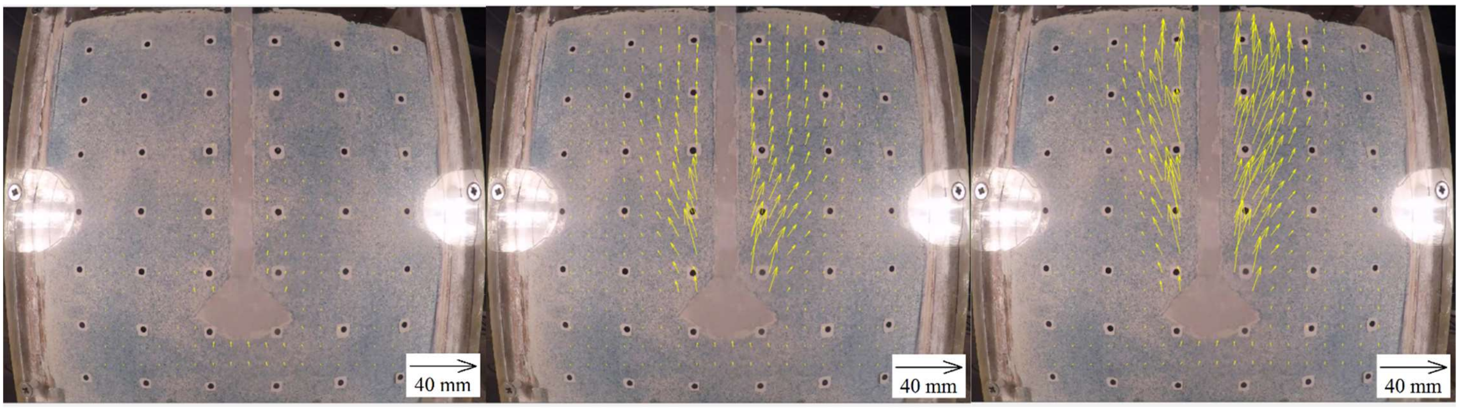

(a) (b) (c)

Figure 33: Progressive PIV vector plots for 45° under-reamed pile in stiff clay
(a) Small strain, $\frac{\delta}{B} \approx 0.01$; (b) Peak, $\frac{\delta}{B} \approx 1.08$; (c) Post-peak, $\frac{\delta}{B} \approx 2.02$

Again the failure mechanisms here were largely common to those of a plate anchor in stiff clay, hence description given in section 5.1.2 is equally applicable in this case. The underlying failure mechanism observed can be used to characterise various regimes of the pile load-displacement behaviour.

Any tension cracks initiated will extend upwards as the pile rises towards the ground surface, i.e. failure is progressive. This forms the physical basis of the slight softening behaviour featured in regime 4. It was noticed by visual inspection that these cracks propagated faster under a given rate of upward displacement in stiff than soft clay, thus explaining the steeper drop in post-peak capacity onto a plateau (regime 4) for curves 4 and 5 compared to curve 3 (Figure 18).

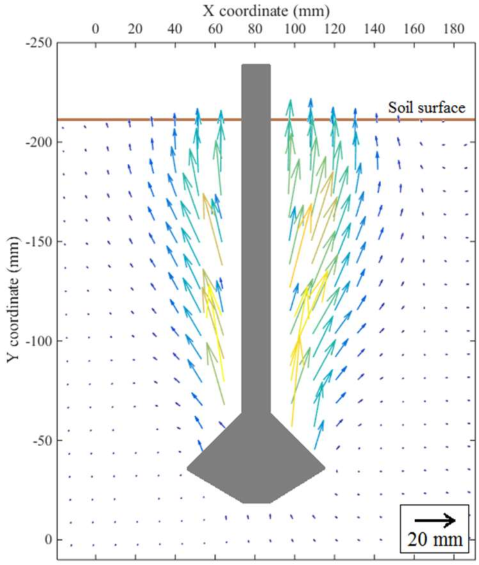

Figure 34: Cumulative PIV vector plot for 45° under-reamed pile in stiff clay

When the tension cracks became fully developed reaching the ground surface, a soil wedge bounded by these cracks (usually in the shape of a concave cone) was lifted up and stressed mostly in flexure. The soil wedge therefore tried to move away from the pile shaft (Figure 35). Subsequently, as progressively less soil was being sheared, the pile load decreased markedly. This was believed to be the physical event corresponding to regime 5 (strain softening at very large displacements). The enormous amount of compression experienced by the soil could be inferred from Figure 35 by comparing the small amount of soil surface heave against the large distance over which the pile had moved.

Figure 35: Failure soil wedge with fully developed tension cracks elevation view (left); top view (right)

5.2.3 Dense sand mechanism

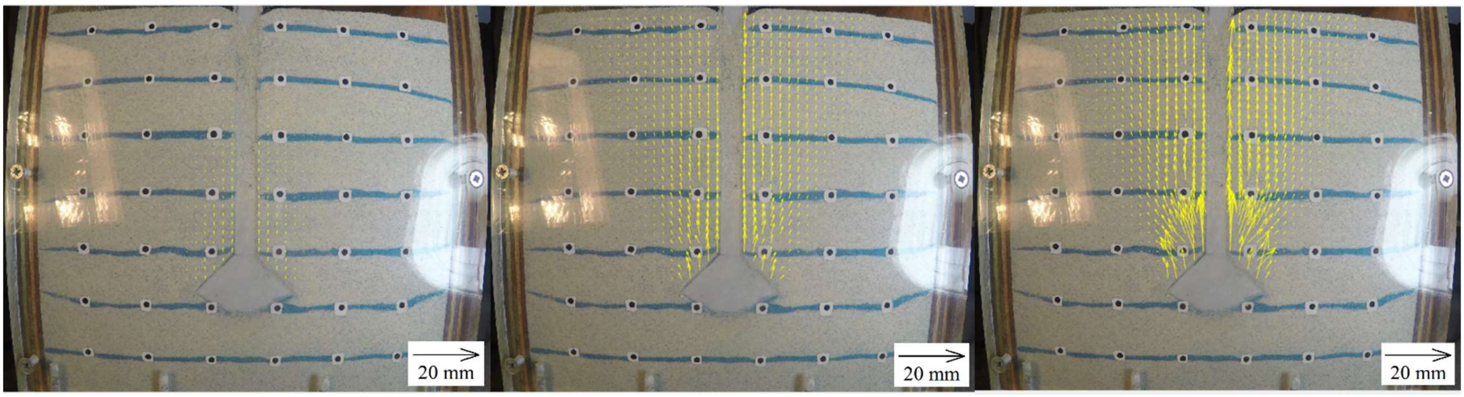

(a) (b) (c)

Figure 36: Progressive PIV vector plots for 45° under-reamed pile in dense sand
(a) Small strain, $\frac{\delta}{B} \approx 0.01$; (b) Peak, $\frac{\delta}{B} \approx 0.03$; (c) Post-peak, $\frac{\delta}{B} \approx 0.08$

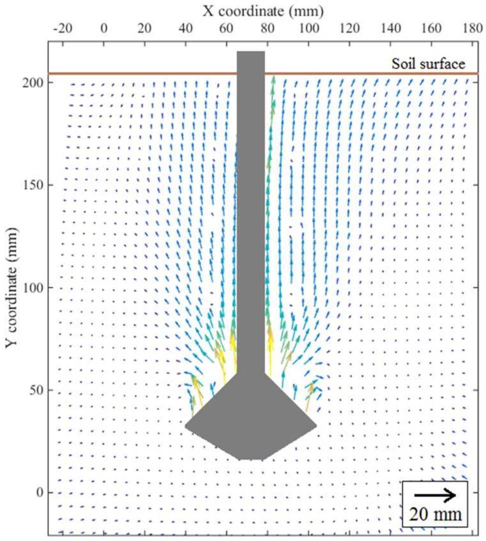

Figure 37: Cumulative PIV vector plot for 45° under-reamed pile in dense sand

With small imposed displacements, resistance was only mobilised in a confined cylindrical soil column with the width of the under-ream (Figure 36(a)). This short soil column was displacing vertically upwards as all vectors shown are pointing upwards without rotation. This developed into a conical failure mechanism at peak capacity with the displacements reaching the ground surface (Figure 36(b)). At this stage, movement of the pile was still relatively small ($\frac{\delta}{B} \approx 0.03$). Onto the post-peak regime, the failure geometry was fully developed with the boundaries of the cone unchanged, i.e. same amount of soil mass inside the conical wedge was involved ever since the peak response (Figure 36(c)). However, for the region immediately above the under-ream, substantial contraction was observed as there was a contrasting variation in vector magnitude within this region, which might be an evidence of the existence of locally loose regions within the sand bed (see section 4.1.3). The rest of the soil inside the cone moved approximately as a rigid wedge. At shallow depths, the vectors became more horizontal approaching the ground surface. This meant that sand in those areas was being displaced horizontally to accommodate for the rising under-ream and sand above it. No movement was observed below the pile base except the effect of soil arching (not considered in the PIV analysis).

5.2.4 Comparison between dense sand and soft/stiff clay mechanisms

Comparing between failure mechanisms of sand and of clay reveals the following differences:

- Initial small-strain mechanism – localised 'deep' mechanisms without reaching the ground surface were observed for both cases. Resistance was mobilised in the form of a short cylindrical soil column above the enlarged base in sand. For clay it was a confined bulb of plastic deformation surrounding the base.
- Ultimate failure mechanism – in sand a well-defined truncated cone (or an inverted frustum) of soil was ruptured in shear, together with some local compaction immediately above the enlarged base. For clay the shape of the overall plastic zone above the base was a convex cone in which soil underwent irreversible movements without rupturing. At shallow depths, the tensile stress in clay eventually led to formation of tension cracks and

flexure of a concave conical soil wedge that was of smaller size than the cone of mobilised sand.

- Displacement to failure – the ultimate failure mechanism was attained at a much smaller applied displacement in sand than in clay, with the respective displacements to failure differing by up to 2 orders of magnitude. It was the high degree of plastic flow involved in clay mechanisms that enabled mobilisation of large displacements.
- Effect below base – there was no movement (and hence no contribution to the uplift capacity) in the soil beneath the pile base in sand, as expected for a granular material. For clay, its cohesive nature was characterised by negative pore pressures (i.e. suction) below the pile base, which significantly affected the resulting pile load-displacement response.

5.2.5 Comparison to literature

For the dense sand mechanism, the conical rupture plane corresponds well to the truncated soil cone model (Figure 5) proposed by Ilamparuthi et al. (2002). Dickin & Leung (1992) also had a similar observation for a 45° under-reamed pile in homogeneous dense sand. The results share many common features with those from a similar PIV analysis conducted by Harris & Madabhushi (2015). The cone angle was found to be roughly 67° to the horizontal, which coincided with the findings by Hughes (2015), and was approximately equal to $90^o - \frac{\phi}{2}$ as noted by Harris & Madabhushi (2015). At shallow depths locations, the displacement vectors had a mean inclination of approximately 8° to the vertical, which was much smaller than the angle between the under-ream surface and the vertical (45° in this case). The displacement vectors immediately above the under-ream were found to deviate from vertical to another angle of 8° on average over the course of the test. This value again coincided with that obtained by Harris and Madabhushi (2015), but not for Hughes (2015) who observed these vectors to be vertical and not at an incline. Merifield & Sloan (2006) concluded in their numerical analysis that no plastic flow occurred below a plate anchor in homogeneous sand at peak response. This proposition is shown in the present study to be applicable to under-reamed piles as well.

A main difference among these results in dense sand is the occurrence of significant local densification in the region immediately above the under-ream, which was not observed by Harris & Madabhushi (2015) in dense sand but in loose sand instead. Moreover, the investigators on the contrary observed some form of cavity expansion in this region, known as the "hemisphere of expansion". This disagreement may be attributed to heterogeneities in the sand model used in the current test, as described in section 4.1.3.

Limited research on the uplift failure mechanism geometry of under-reamed piles in clay has been carried out historically, possibly due to its complexity over failure mechanisms of sand. In this project, most of the results obtained for the plate anchor were found to be applicable in general to under-reamed piles as well, suggesting that as long as the pile base was enlarged, the under-ream angle θ had little effect on the failure mechanism in clay, apart from the base suction phenomenon detailed in section 5.2.1. Even so, the difference in suction observed between the plate anchor and the 45° under-reamed pile (section 5.2.1) was thought to be largely due to the bottom face geometry of the enlarged base specific to this project. For example, piles in other circumstances may well be belled out at 45° yet still have a flat bottom surface, which is common for drilled piers in the U.S (Reese & O'Neill, 1999). In this case, the base suction developed may be similar to that for a plat anchor of the same size in the same clay. Further investigation is required to confirm this since only two different under-ream angles (0° and 45°) were employed in this project. It follows that the clay failure modes suggested by Merifield et al. (2003) would yield similar comparisons for the under-reamed pile as for the plate anchor.

The numerical results of peach-shaped plastic zone contours for a partly-cohesive soil under SLS (small strain) conditions (Figure 8) obtained by Xu et al. (2012) suggested a shape resembling the localised bulb that characterised the small strain failure mechanisms of clay observed in the current study. The latter also appeared to be peach-shaped as indicated by the directions of the displacement vectors – as the pile progressed upwards the soil immediately above the under-ream surface was trying to turn away from the vertical, travel down the sides and head towards the base bottom with a tendency to 'replace' the heaved soil there. This peach-shaped displacement field was similarly observed for the plate anchor and is most clearly shown in Figure 26(a) and Figure 29(a).

On the contrary, the ultimate failure mechanisms observed did not seem to resemble the general failure modes of fully sized belled piers proposed by Tucker (1988) for $\frac{D}{B_s} > 6$. The difference in shape is illustrated in Figure 38. Scale effects may play a role in this discrepancy.

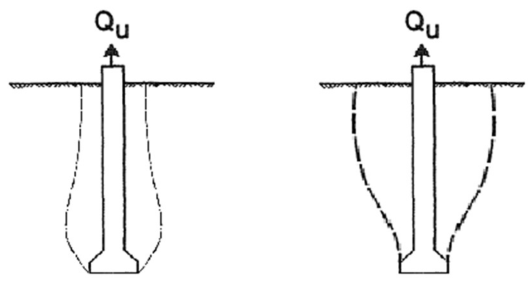

Figure 38: Failure mechanism geometry for belled piers predicted by Tucker (1988) (left) and observed in the current tests (right)

Since the load-displacement behaviour of piles can be explained with the aid of the underlying failure mechanisms, having visualised and examined the soft and stiff clay mechanisms, the discrepancy presented in section 4.2.1 regarding regime 4 of the pile load-displacement response observed in this project and results reported in literature can now be explained on a physical basis. To recap, most researchers presented load-displacement graphs showing an elasto-plastic behaviour ending with a plateau (e.g. Figure 23 and Figure 24), while all four clay tests conducted in this project (tests JL2 to JL5) showed a slight decrease in pile capacity after the ultimate state followed by a later temporary plateau (regime 4), which was believed to be caused by the propagation of tension cracks towards the soil surface (section 5.2.2).

For numerical results it is reasonable to believe that the formation and development of these cracks were usually not modelled in the simulations because of the difficulty and variability involved in doing so. For experimental results, depending on the nature of the tests conducted, load-controlled tests simply would not capture any softening behaviour, while for displacement-controlled tests it is thought that most researchers did not continue their tests to displacements as large as the current tests (up to $\frac{\delta}{B} \approx 2$) for various reasons such as limits of test equipment (Chaudhuri & Symons, 1986) and constraints on test duration. This implies the failure mechanism remained ‘deep’ and localised at all times during the tests, any features regarding tension cracks would thus not be discovered. A similar argument was applied in section 4.2.3 to explain the non-existence of the falling branch at very large displacements (regime 5) in most published results.

6. Theoretical Predictions

In this chapter, several generalised methods for estimating the ultimate uplift capacity of under-reamed foundations in homogeneous clay are briefly summarised and compared against results from the current tests. Notation for various parameters is as defined using the nomenclature in this report unless specified otherwise.

6.1 Theoretical model by Meyerhof & Adams (1968) and its variants

Meyerhof & Adams (1968) suggested that the short-term (undrained) uplift capacity for deep anchors in clay would be the lesser of the base resistance offered by the under-ream (Q_b) and the shaft resistance (Q_s). For the former, they predicted that it would be related to the undrained shear strength c_u and analogous to the bearing capacity:

$$Q_b = Ac_uN_u + W \tag{1}$$

where N_u is an uplift coefficient ≈ 9 at an embedment ratio of $\frac{D}{B}$ = 3 and W is the combined weight of the pile and the cylindrical soil column above the enlarged base. Poulos & Davis (1980) suggested a modification to equation (1) for the case of under-reamed piles by considering only the projected annular area between the under-ream and the pile shaft:

$$Q_b = \left(\frac{\pi}{4}\right)(B^2 - {B_s}^2)c_uN_u + W \tag{2}$$

For the shaft resistance, cylindrical theory is commonly assumed, i.e. shaft friction would be mobilised along a cylindrical surface above the base and within the diameter of the under-ream:

$$Q_s = \Psi\pi B'L_ec_u + W \tag{3}$$

where B' is the effective diameter of the cylindrical surface, L_e is the effective pile length over which shaft friction is mobilised and Ψ is an empirical correction factor for the undrained strength c_u of different clay types. Researchers had different interpretations of this cylinder, regarding its diameter B', length L_e and the factor Ψ. These are summarised in Table 5.

Table 5: Various interpretations of cylindrical surface mobilised to generate shaft resistance

Reference	B'	L_e	Ψ
Poulos & Davis (1980)	B	D	Soft clays: 1 Stiff clays: 0.5
Tucker (1988) (Figure 39(a))	$B_s + \frac{1}{3}(B - B_s)$	D	1
Prakash & Sharma (1990) (Figure 39(b))	$\frac{1}{2}(B + B_s)$	D	1
Reese & O'Neill (1999) (Figure 39(c))	B_s	$D - \frac{1}{2}(B - B_s)\tan\theta - 2B$	0.55

The ultimate uplift capacity is then given by the lesser of equations (2) and (3).

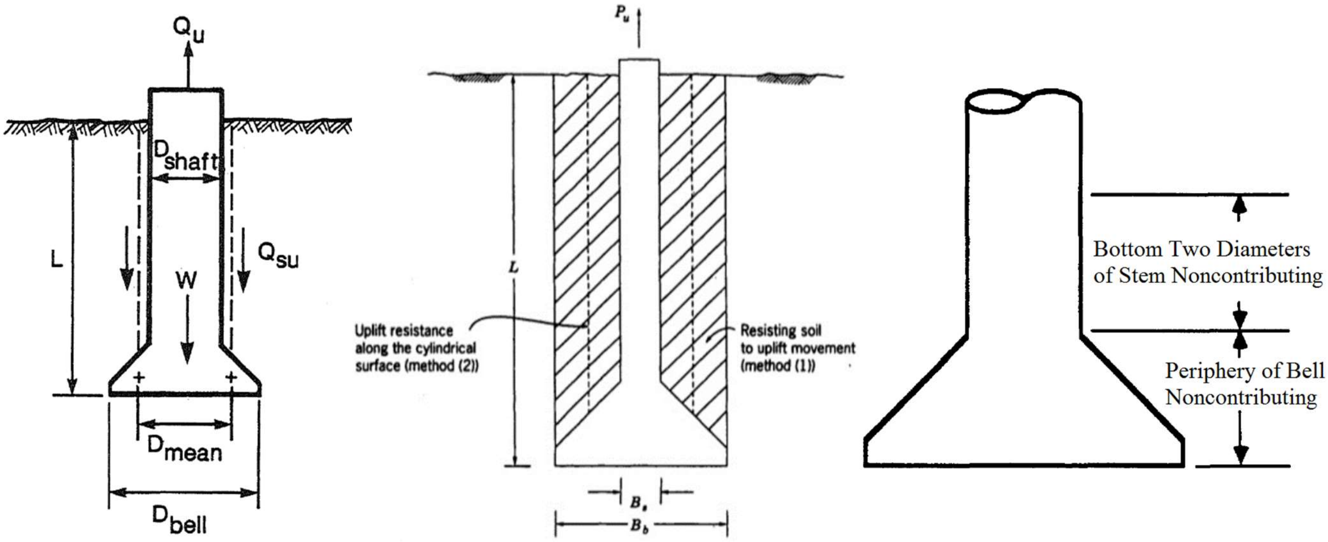

Figure 39: (a) Equivalent force diagram for determining uplift shaft resistance of belled piers (Tucker, 1988)
(b) Schematic for determining ultimate uplift capacity of belled piles (Prakash & Sharma, 1990)
(c) Exclusion zones for determining uplift shaft resistance of drilled piers in cohesive soils (after Reese & O'Neill,1999)

6.2 Estimation procedure by Das (1980)

Based on model test results, a generic routine to estimate the ultimate uplift capacity of plate anchors embedded in clay was proposed by Das (1980). This method was claimed to be applicable to foundations of any regular shape (circular, square or rectangular) in any clay (with different values of c_u). For circular anchors, the procedure is outlined in the following:

1. Evaluate the critical embedment ratio: $\left(\frac{D}{B}\right)_{cr} = 0.107c_u + 2.5 \leq 7$ (c_u in kPa) (4)
2. Take the breakout factor F_c^* to be equal to the bearing capacity factor for deep anchors recommended by Vesic (1971) and Meyerhof & Adams (1968): $F_c^* = 9$
3. Evaluate the breakout factor F_c corrected for embedment. For deep anchors, $\left(\frac{D}{B}\right) \geq \left(\frac{D}{B}\right)_{cr}$, adopt $F_c = F_c^*$. For shallow anchors, $\left(\frac{D}{B}\right) \leq \left(\frac{D}{B}\right)_{cr}$, adopt $F_c = \beta F_c^*$ where β is determined from α using a plot, and $\alpha = \frac{D/B}{(D/B)_{cr}}$.
4. Evaluate the net ultimate uplift capacity: $Q_o = B^2(F_c c_u + \gamma D)$ (5)
5. Determine the gross ultimate uplift capacity: $Q_u = Q_o + W_p$ (6)
   where W_p is the weight of the pile anchor.

6.3 3D lower bound solutions by Merifield et al. (2003)

Another procedure for estimating the ultimate uplift capacity of plate anchors in clay was suggested by Merifield et al. (2003) on the basis of an extensive finite element formulation on various plate geometries including circular, square and rectangular anchors. The procedure is outlined below again for the case of rough circular anchors:

1. Take the limiting breakout factor $N_c^* = 12.56$ as found from FE lower bound analyses.
2. Evaluate the breakout factor for weightless soil: $N_{co} = S\left[2.56\, ln\left(2\frac{D}{B}\right)\right]$ (7)

   where S is a shape factor determined from $\frac{D}{B}$ using a plot.
3. Evaluate the breakout factor corrected for soil unit weight: $N_{c\gamma} = N_{co} + \frac{\gamma D}{c_u}$ (8)
4. Evaluate the breakout factor N_c corrected for embedment. For deep anchors, $N_{c\gamma} \geq N_c^*$, adopt $N_c = N_c^*$. For shallow anchors, $N_{c\gamma} \leq N_c^*$, adopt $N_c = N_{c\gamma}$.
5. Determine the ultimate uplift capacity: $Q_u = Ac_uN_c$ (9)

6.4 Analytical equation by Golait et al. (2014)

Golait et al. (2014) established an analytical equation for estimating the ultimate pullout capacity of under-reamed piles in soft to medium clays, which was derived by considering equilibrium in a conceptual load transfer failure mechanism along with some idealisations (Figure 40). The final equation and the assumed mechanism are simply quoted here for brevity:

$$\begin{cases} Q_u = \pi c_u[0.9B^2 + \alpha B_s(D - 0.9B)] + \pi\gamma\left[\frac{H^3 tan^2\beta}{3} - \frac{B^3}{24tan\beta} - \frac{B_s{}^2(D-0.9B)}{4}\right] + W_p \\ H = \frac{B+2Dtan\beta-1.8Btan\beta}{2ta} \end{cases} \quad (10)$$

where α is the shaft adhesion factor taken to be 0.5 as recommended by the Indian Standard Code of Practice (Bureau of Indian Standards, 1980), β is the idealised cone angle to the vertical for which $\begin{cases} \beta = 24°, \frac{D}{B_s} \leq 10 \\ \beta = 22°, \frac{D}{B_s} > 10 \end{cases}$ and W_p is the weight of the pile.

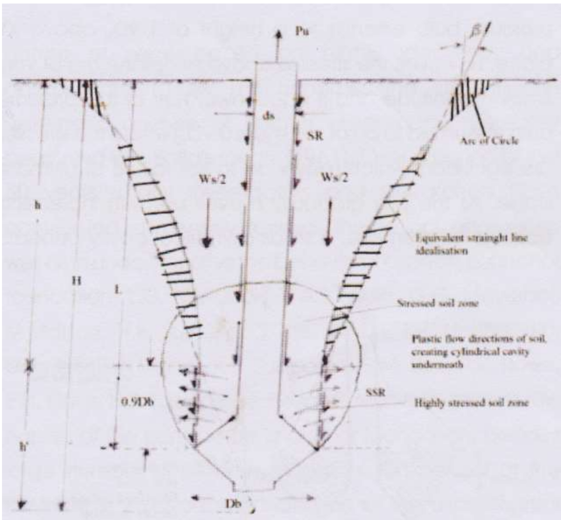

Figure 40: Assumed failure mechanism for soft to medium clays (Golait et al., 2014)

6.5 *Comparison with experimental results*

The aforementioned predictions were applied to the current test scenarios, and were compared against the actual results obtained from tests JL2 to JL5 in clay. This is illustrated in Figure 41.

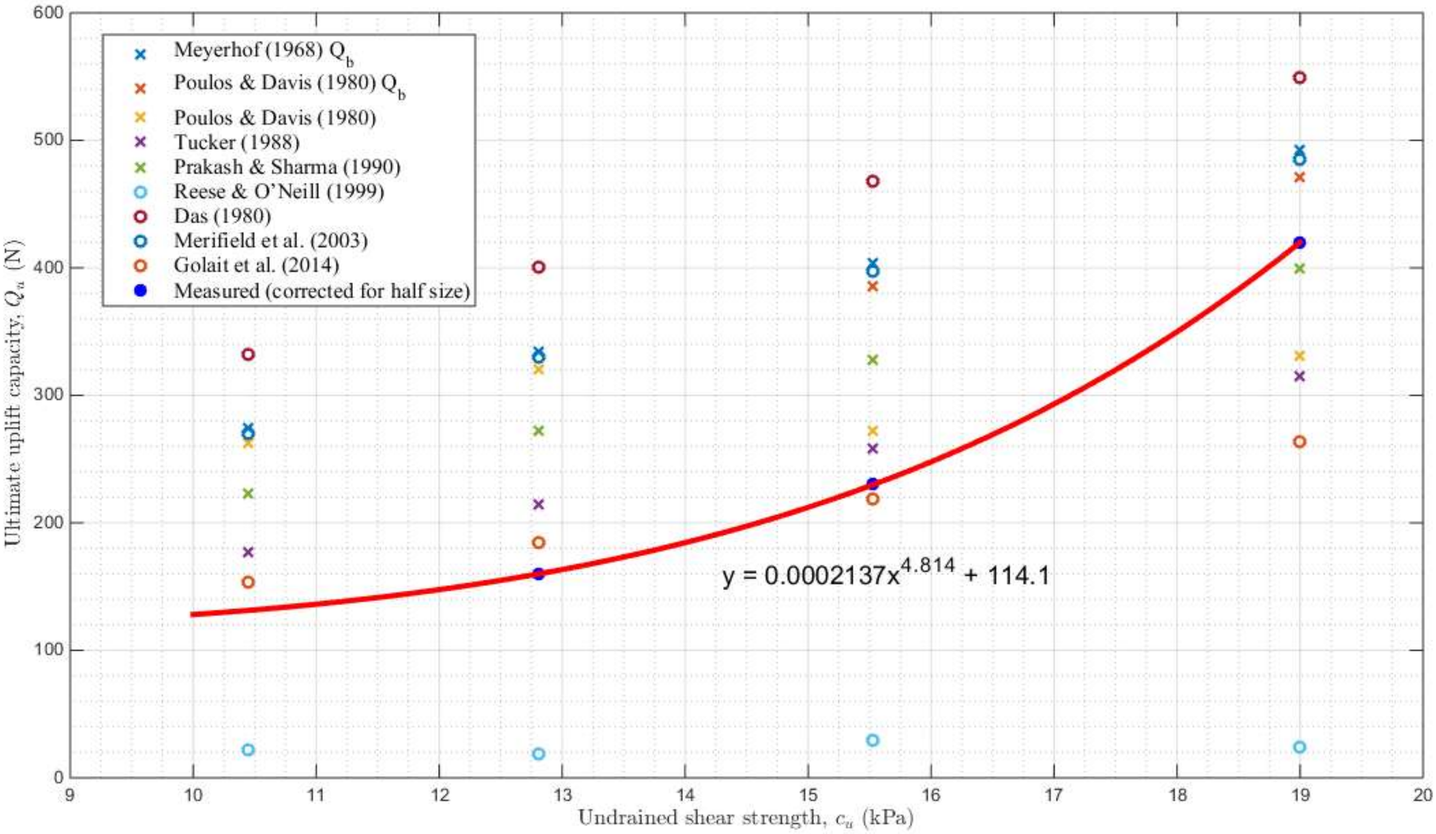

Figure 41: Summary plot of various theoretical predictions and actual test results of ultimate uplift capacity of under-reamed piles in clay

Figure 41 depicts an overall trend of ultimate uplift capacity increasing with undrained strength c_u across the tests as logically expected, with an exception for the method proposed by Poulos & Davis (1980). This is due to the fact that the clays used in the current project were arbitrarily classified as 'soft' and 'stiff' in view of their relative consistencies, while this decision would have a significant effect on the resulting value of Q_u. The shaft resistance in stiff clays is only half of that in soft clays due to the development of tension cracks in the former to premature failure. The size-dependent estimates by Reese & O'Neill (1999) are proven to be over-conservative for small scale model piles. Prediction by Golait et al. (2014) yields the closest results as the assumed failure mechanism was derived from similar model tests conducted in soft to medium clays. Thus, it can be seen that the prediction starts to deviate with stiffer clays. Overall, the methods are mostly suitable or conservative for stiff clays but they tend to overestimate the capacity in soft clays. Some of the methods (Das, 1980; Merifield et al., 2003) even assume no base suction and yet still appear to be unconservative. Therefore, all these methods have to be used with caution when designing under-reamed piles in soft clays.

7. Conclusions

Current test results indicated that the uplift load-displacement response of under-reamed piles in dense sand resembled the expected behaviour of such soil upon shearing, whereby the sand initially dilates, reaches a well-defined peak strength at a relatively small displacement, then softens post-peak towards a critical state. Post-failure instability due to soil arching was noticeable. The associated failure mechanism was a truncated cone ruptured in shear with some local compaction immediately above the base.

For clay, five regimes of behaviour were identified, each characterised by various stages of the underlying failure mechanism. At small strains (regime 1), the capacity increased rapidly and the initial stiffness increased with undrained shear strength via a power-law relation. Yielding (regime 2) then followed, mobilising large displacements towards the ultimate state (regime 3). The peak capacity was observed to increase with undrained strength described by another power-law relation. Up to this point, a growing localised plastic zone in the form of a peach-shaped bulb was observed around the pile base, together with suction generated beneath the base but lost at an early stage. Sudden dips in load due to the loss of suction at the breakaway state were observed for the plate anchor but not for the 45° under-reamed pile because of the different base bottom profile, in which a flat surface was more prone to abrupt breakaway. The loss of suction caused degradation in both stiffness and capacity. For load-controlled scenarios a dynamic jump in displacement would occur during breakaway, which might cause unpredictable damage to any overlying structures. Subsequently, the post-peak capacity was found to decrease slightly towards a temporary plateau (regime 4), reflecting the initiation and extension of tension cracks at shallow depths starting from the rim of the pile base towards the soil surface. For stiff clays, faster crack propagation led to a steeper fall in capacity. At very large displacements, the clay exhibited strain softening (regime 5) as the cracks became fully-developed reaching the soil surface. A concave conical wedge defined by these cracks was then stressed largely in flexure and lifted up, causing the soil surface around the pile shaft to heave.

Comparisons between results in clay and in sand revealed that the former exhibited a much higher degree of plasticity, as expected for purely cohesive soils compared to frictional, granular soils. Several generalised methods for predicting the ultimate uplift capacity of under-reamed piles embedded in clay were discussed and compared against current test results. The methods were found to be mostly suitable or conservative for stiff clays, but they tended to overestimate the capacity in soft clays. Consequently, all these methods have to be used with caution in design.

8. Recommendations for Future Work

The uplift behaviour of under-reamed piles (particularly in clay) is nowhere near to be fully understood. Hence, to further investigate this subject, small scale model testing at 1g is useful as it can be performed with relative ease. Suggestions on this include:

- Varying the embedment ratio $\frac{D}{B}$ across tests to characterise pile response into 'deep' and 'shallow' regimes and assess the concept of critical embedment ratios proposed by Meyerhof & Adams (1968). Most historical investigations on uplift capacity were done in the depth domain, providing a large database for any comparisons of results to be made.
- Employing model piles with a range of under-ream geometries, e.g. different under-ream angles θ, base profile (flat, slanted or round), location (at the base or at an intermediate position along the pile stem) and amount in a pile (single or multiple). These are expected to have an effect on both the uplift capacity and failure mechanism geometry.
- Testing more samples of Kaolin clay and other clay species with a wider range of c_u. Much of the soil properties was unknown in this project (section 3.2.2), making it difficult to correlate with the results. If time permits, the clay bed should be prepared from scratch to get a better grasp of the stress history and properties of the test soil, as these might significantly affect the pile uplift behaviour and soil failure mechanism. Although difficulty in doing so was well realised (Chaudhuri & Symons, 1986).
- Testing in layered, heterogeneous (e.g. c_u linearly increasing with depth), composite and expansive strata which are prevalent in field conditions. There might be difficulties to simulate swelling of expansive soils in a test though.
- Examining rate effects and suction in clay. Suction can be quantified by pore pressure measurement via pore pressure transducers and control tests in which suction is prevented at all times (e.g. by introducing a base drainage layer of sand or non-cohesive lining under the pile base). As undrained conditions become drained over time, overlooking the dissipation of negative pore pressures under sustained loading could lead to dangerous overestimation of capacity in design (Meyerhof & Adams, 1968).
- Investigating common scenarios in practice, e.g. pile group effects and inclined loading.

However, due to scale effects (difference in soil confining stress levels), centrifuge testing at elevated gravities is preferable as small scale tests tend to yield unconservative results for the field (Dickin & Leung, 1990). Full-scale field tests are deemed necessary for final design (Chaudhuri & Symons, 1986; Prakash & Sharma 1990; Su et al., 2006). Finally, numerical analyses allow copious simulations to be run, saving time and any practical experiment costs.

References

Balla, A., 1961. "The Resistance of Breaking Out of Mushroom Foundations for Pylons", *Proceedings of the 5th International Conference on Soil Mechanics and Foundation Engineering.* Paris, 17-22 July 1961. Paris: Dunod, pp.569-576.

Bureau of Indian Standards, 1980. *IS:2911-3: Code of Practice for Design and Construction of Pile Foundations: Under-Reamed Piles.* New Delhi: Bureau of Indian Standards.

Chai, J. C., Carter, J. P. & Hayashi, S., 2005. "A Method for Modeling Strain-Softening Behavior of Clay and its Application for Simulating Uplift Resistance of a Belled Foundation", *Proceedings of the 2nd Sino-Japanese Geotechnical Symposium.* Shanghai, China. Tongji University Press, pp.167-174.

Chaudhuri, K. P. R. & Symons, M. V., 1986. "Uplift Resistance of Single Model Piles in Clay", *Proceedings of the 3rd International Conference on Numerical Method in Offshore Piling*. Nantes, 21-22 May 1986. Paris: Technip, pp.495-510.

Das, B. M., 1978. "Model Tests for Uplift Capacity of Foundations in Clay", *Soils and Foundations, Journal of the Japanese Society of Soil Mechanics and Foundation Engineering*, Vol.18 No.2, pp.17-24.

Das, B. M, 1980. "A Procedure for Estimation of Ultimate Uplift Capacity of Foundations in Clay", *Soils and Foundations, Journal of the Japanese Society of Soil Mechanics and Foundation Engineering*, Vol.20 No.1, pp.77-82.

Dickin, E. A, 1988. "Uplift Behaviour of Horizontal Plate Anchors in Sand", *Journal of Geotechnical Engineering*, Vol.144 No.11, pp.1300-1317.

Dickin, E. A. & Leung, C. F., 1990. "Performance of Piles with Enlarged Bases Subject to Uplift Forces", *Canadian Geotechnical Journal,* Vol.27 No.5, pp.546-556.

Dickin, E. A. & Leung, C. F., 1992. "The Influence of Foundation Geometry on the Uplift Behaviour of Piles with Enlarged Bases", *Canadian Geotechnical Journal,* Vol.29 No.3, pp.498-505.

Golait, Y. S., Dahale, P. & Jiwatode, R. N., 2014. "Analytical and Experimental Studies on Underreamed Pile as Anchor Foundation in Soft Clay". *i-manager's Journal on Civil Engineering*, Vol.4 No.3, pp.25-32.

Gupta S., 1986. "For Which Soil Conditions Are Under-Reamed Pile Foundations Superior to Other Foundations Systems?", Synthesis Paper, *Proceedings of the Indian Geotechnical Conference 1986.* New Delhi. Vol.2, pp.97-101.

Harris, D. E., 2014. "Uplift Resistance of an Under-Reamed Piled Foundation", PR. CUED: Fourth Year Undergraduate Project Report.

Harris, D. E. & Madabhushi, S. P. G., 2015. "Uplift Capacity of an Under-Reamed Pile Foundation", accepted by *Proceedings of the ICE – Geotechnical Engineering,* Thomas Telford, London.

Hopkins, A., 2012. "The Uplift Capacity of Under-Reamed Piles", PR. CUED: Fourth Year Undergraduate Project Report.

Hughes, F. E., 2015. "Uplift Resistance of an Under-Reamed Pile Foundation", PR. CUED: Fourth Year Undergraduate Project Report.

Ilamparuthi, K., Dickin, E. A. & Muthukrisnaiah, K., 2002. "Experimental Investigation on the Uplift Behaviour of Circular Plate Anchors Embedded in Sand", *Canadian Geotechnical Journal,* Vol.39 No.3, pp.648-664.

Jain, G. S., Sharma, D. & Prakash, C., 1975. "Bored Compaction Piles", *Building Digest*. Roorkee, India: Central Building Research Institute, No.116.

Lehane, B. M., Gaudin, C., Richards, D. J. & Rattley, M. J., 2008. "Rate Effects on the Vertical Uplift Capacity of Footings Founded in Clay". *Géotechnique*, Vol.58 No.1, pp.13-21.

Merifield, R. S., Lyamin, A. V., Sloan, S. W. & Yu, H. S., 2003. "Three-Dimensional Lower Bound Solutions for Stability of Plate Anchors in Clay", *ASCE Journal of Geotechnical and Geoenvironmental Engineering*, Vol.129 No.3, pp.243-253.

Merifield, R. S. & Sloan, S. W., 2006. "The Ultimate Pullout Capacity of Anchors in Frictional Soils", *Canadian Geotechnical Journal*, Vol.43 No.8, pp.852-868.

Meyerhof, G. G., 1951. "The Ultimate Bearing Capacity of Foundations", *Géotechnique*, Vol.2, pp.301-332.

Meyerhof, G. G. & Adams, J. I., 1968. "The Ultimate Uplift Capacity of Foundations", *Canadian Geotechnical Journal*, Vol.5 No.4, pp.225-244.

Mitrani, H., 2006. "Liquefaction Remediation Techniques for Existing Buildings". CUED: PhD Thesis.

Mohan, D., 1989. "Economical Piling in Soft Soils and Expansive Clays", *Piling and Deep Foundations: Proceedings of the International Conference on Piling and Deep Foundations.* London, 15-18 May 1989. Rotterdam: Balkema, Vol.1, pp.79-83.

Murray, E. J. & Geddes, J. D., 1987. "Uplift of Anchor Plates in Sand", *Journal of Geotechnical Engineering*, Vol.113 No.3, pp.202-215.

Poulos, H. G. & Davis, E. H., 1980. *Pile Foundation Analysis and Design*. New York: John Wiley and Sons, pp.44-48.

Prakash, S. & Sharma, H. D., 1990. *Pile Foundations in Engineering Practice*. New York: John Wiley and Sons, pp.18-19,305-321.

Rattley, M. J., Richards, D. J. & Lehane, B. M., 2008. "Uplift Performance of Transmission Tower Foundations Embedded in Clay", *ASCE Journal of Geotechnical & Geoenvironmental Engineering*, Vol.134 No.4, pp.531-540.

Reese, L. C. & O'Neill, M. W., 1999. *Drilled Shafts: Construction Procedures and Design Methods,* Report No. FHWA-IF-99-025. Washington D.C.: Federal Highway Administration, U.S. Department of Transportation, pp.262-296.

Rowe, R. K. & Davis, E. H., 1982. "The Behavior of Anchor Plates in Clay.", *Géotechnique*, Vol.32 No.1, pp.9-23.

Sakajo, S., Chai, J. C., Yoshimaru, T. & Kamimura, M, 1995. "Prediction Analyses of Up-lift Resistance of a Belled Foundation in Cohesive Soil, *Proceedings of the 5th International Symposium on Numerical Models in Geomechanics*. Davos, Switzerland. Rotterdam: Balkema, pp.595-599.

Sharma, D., Jain, M. P. & Prakash, C., 1978. *Handbook on Under-Reamed and Bored Compaction Pile Foundations*. Roorkee, India: Central Building Research Institute.

Singh, S. P. & Ramaswamy, S. V., 2008. "Effect of Shape on Holding Capacity of Plate Anchors Buried in Soft Soil", *Geomechanics and Geoengineering: An International Journal.* Abingdon: Taylor & Francis, Vol.3 No.2, pp.157-166.

Stanier, S. A., Blaber, J., Take, W. A. & White, D. J., 2015. "Improved Image-Based Deformation Measurement for Geotechnical Applications", *Canadian Geotechnical Journal*, Vol.53 No.5, pp.727-739.

Su, H., Li, Q. F. & Li, Y. J., 2006. "Analysis and Research for Uplift Mechanism on Foundation of Transmission Line Towers in Expansive Soil", *Journal of the Institute of Rock and Soil Mechanics.* Wuhan, China: Chinese Academy of Sciences, Vol.27 No.8, pp.1411-1415. (in Chinese)

Sutherland, H. B., 1988. "Uplift Resistance of Soils", *Géotechnique*, Vol.38 No.4, pp.493-516.

Tand, K. E., Vipulanandan, C. & O'Neill, M. W., 2005. "Load-Displacement Behavior of Underreamed Footings Bearing in Jointed Clays". Available at: www.gemsoft.us/Papers/Underreamed%20Footings%20in%20Jointed%20Clay.pdf, [Date last accessed: 15/05/2016]

Thorne, C. P., Wang, C. X. & Carter, J. P., 2004. "Uplift Capacity of Rapidly Loaded Strip Anchors in Uniform Strength Clay", *Géotechnique*, Vol.54 No.8, pp.507-517.

Tomlinson, M. J., 2001. *Pile Design and Construction Practice*, 4th ed. London: Spon Press, pp.79-82.

Tucker, K. D., 1987. "Uplift Behaviour of Drilled Shaft and Driven Piles in Granular Soils", *Foundations for Transmission Line Towers.* New York: ASCE Geotechnical Special Publication, No.8, pp.142-159.

Tucker, K. D., 1988. "Performance Evaluation of Pile Foundation Using CPT Data", *Proceedings of the 2nd International Conference on Case Histories in Geotechnical Engineering*. St. Louis, Missouri, 1-5 June 1988. Paper No. 6.58.

Varghese, P.C., 2009. *Design of Reinforced Concrete Foundations.* New Delhi: PHI Learning Private, pp.227-235.

Vesic, A. S., 1971. "Breakout Resistance of Objects Embedded in Ocean Bottom", *Journal of the Soil Mechanics and Foundations Division*, Vol.97 No.9, pp.1183-1205.

White, D. J. & Take, W. A., 2002. "GeoPIV: particle image velocimetry (PIV) software for use in geotechnical testing". CUED: Technical Report.

White, D. J., Take, W. A. & Bolton, M. D., 2003. "Soil Deformation Measurement Using Particle Image Velocimetry (PIV) and Photogrammetry", *Géotechnique*, Vol.53 No.7, pp.619-631.

Xu, H. F., Yue, Z. Q. & Qian, Q. H., 2009. "Predicting Uplift Resistance of Deep Piles with Enlarged Bases", *Proceedings of the ICE – Geotechnical Engineering*, Thomas Telford, London. Vol.162 No.4, pp.225-238.

Xu, H. F., Yue, Q. Z. Q. & Qian, Q. H., 2012. "Failure Model of Soil Around Enlarged Base of Deep Uplift Piles", *Proceedings of the ICE – Geotechnical Engineering*, Thomas Telford, London. Vol.165 No.5, pp.275-288.

Appendix: Risk Assessment Retrospective

Before the commencement of experimental work, a full risk assessment was undertaken, in addition to the mandatory induction at the Schofield Centre laboratory and the completion of a Project Approval Document (PAD) which sets control measures for safe working specifically at the Centre. Any laboratory work in the Centre must be carried out in accordance with the PAD signed by an authorised engineer. Table 6 summarises the hazards identified and corresponding control measures adopted during the course of the project.

Table 6: Hazards and control measures within project duration

Hazard	Control Measure(s)
<u>Electrical – Data acquisition system</u> Electrical hazards for the user.	Handle with due care and safety precautions.
<u>Mechanical – 1D actuator</u> Multiple moving parts and substantial weight. Potential injuries from misuse for the user.	Only physically handle the actuator when the power supply is turned off, and control it remotely during experiments.
<u>Other – Dust</u> Dust is typically given off when pouring sand. Could cause respiratory issues if inhaled for anyone nearby.	Wear a respirator helmet provided by the Schofield Centre whenever sand is being poured, and carry out all pouring in a sealed room and use dust extractors.
<u>Other – Transportation of heavy items</u> Sand bags and heavy experimental equipment have to be lifted and moved during test preparation. Potential injuries from incorrect lifting and transport procedures for the operators.	Employ correct lifting procedure. Any equipment deemed unsafe to carry alone should be moved using a pallet truck or with the help of another individual. If necessary, the equipment could be transported using a forklift truck, which is to be done by a trained operator at all times.
<u>Other – Computer use</u> Ergonomic issues with prolonged use of computer systems for the user.	Adopt correct seating postures, use a good seat with support, and take breaks during long periods of computer analysis and report writing.

All hazards encountered in this project were successfully reflected in the risk assessment to a high degree of accuracy. There were neither injuries sustained nor near-misses occurred throughout the project.

In view of the thoroughness, adequacy and accuracy of the risk assessment conducted, it is recommended to assess risk in the same manner if the project were to be started over again.